1998

Wafer bonding for fabrication of three-dimensional photonic band gap crystals

Shi-Di Cheng
Iowa State University

INFORMATION TO USERS

This manuscript has been reproduced from the microfilm master. UMI films the text directly from the original or copy submitted. Thus, some thesis and dissertation copies are in typewriter face, while others may be from any type of computer printer.

The quality of this reproduction is dependent upon the quality of the copy submitted. Broken or indistinct print, colored or poor quality illustrations and photographs, print bleedthrough, substandard margins, and improper alignment can adversely affect reproduction.

In the unlikely event that the author did not send UMI a complete manuscript and there are missing pages, these will be noted. Also, if unauthorized copyright material had to be removed, a note will indicate the deletion.

Oversize materials (e.g., maps, drawings, charts) are reproduced by sectioning the original, beginning at the upper left-hand corner and continuing from left to right in equal sections with small overlaps. Each original is also photographed in one exposure and is included in reduced form at the back of the book.

Photographs included in the original manuscript have been reproduced xerographically in this copy. Higher quality 6" x 9" black and white photographic prints are available for any photographs or illustrations appearing in this copy for an additional charge. Contact UMI directly to order.

UMI

A Bell & Howell Information Company
300 North Zeeb Road, Ann Arbor MI 48106-1346 USA
313/761-4700 800/521-0600

Wafer bonding for fabrication of three-dimensional photonic band gap crystals

by

Shi-Di Cheng

A dissertation submitted to the graduate faculty

in partial fulfillment of the requirements for the degree of

DOCTOR OF PHILOSOPHY

Major: Electrical Engineering (Microelectronics)

Major Professor: Gary Tuttle

Iowa State University

Ames, Iowa

1998

Graduate College
Iowa State University

This is to certify that the Doctoral dissertation of

Shi-Di Cheng

has met the dissertation requirements of Iowa State University

Signature was redacted for privacy.

Major Professor

Signature was redacted for privacy.

For the Major Program

Signature was redacted for privacy.

For the Graduate College

TABLE OF CONTENTS

I. INTRODUCTION

I.1. Photonic Band Gap Crystals

Photonic band gap (PBG) crystals are artificially engineered periodic dielectric structures which exhibit frequency regions in which electromagnetic (EM) waves cannot propagate in certain directions. The behavior of electromagnetic waves in such modulated dielectric structures can be viewed as analogous to the behavior of electrons propagating in a periodic lattice potential in crystals. The Bragg-like diffraction from periodic arrangements of atoms or molecules in semiconductors opens up forbidden energy band gaps. Similarly, in photonic band gap crystals, the destructive interference of multiple scattering at the dielectric interfaces (or scattering centers) gives rise to frequency gaps in photon energy bands. Since the concept of photonic band gap crystals was first proposed by Eli Yablonovitch in 1987 [1], these structures have received considerable attention theoretically and experimentally [2, 3] due to their potential uses over a broad frequency range, extending from microwave to optical regimes.

The similarity between electrons in a potential energy, V(r) and an electric field, $\vec{E}(\vec{r})$ of EM waves in an inhomogeneous and absorptionless dielectric material can be shown in Schrödinger equation (1) and EM wave equations (2) and (3), respectively,

$$-\frac{\hbar^2}{2m}\nabla^2\psi(\vec{r}) + V(\vec{r})\psi = E\psi(\vec{r}) \tag{1}$$

$$\nabla\times\left(\nabla\times\vec{E}(\vec{r})\right) = \varepsilon(\vec{r})\left(\frac{\omega}{c}\right)^2\vec{E}(\vec{r}) \tag{2}$$

or

$$-\nabla^2\vec{E}(\vec{r}) + \nabla(\nabla\cdot\vec{E}(\vec{r})) - (\varepsilon(\vec{r}) - \varepsilon_0)\frac{\omega^2}{c^2}\vec{E}(\vec{r}) = \varepsilon_0\frac{\omega^2}{c^2}\vec{E}(\vec{r}) \tag{3}$$

In the Schrödinger equation (1), m is the mass of electron, $\psi(r)$ is electron wave function, and E is eigenenergy. In the wave equations (2) and (3), the dielectric constant, $\varepsilon(\vec{r})$, of the inhomogeneous material is real and positive with an averaged value of ε_0. It is clear that the EM wave equation (eigen equation) is equivalent to Schrödinger equation with following substitutions.

$$V(\vec{r}) \Rightarrow (\varepsilon(\vec{r}) - \varepsilon_0)\frac{\omega^2}{c^2},$$

$$E \Rightarrow \varepsilon_0 \frac{\omega^2}{c^2}$$

and

$$\psi(\vec{r}) \Rightarrow \vec{E}(\vec{r}).$$

Due to the similarities between semiconductor crystals and photonic periodic system, many likewise properties have been observed.

I.2. General Properties of Photonic Band Gap Crystals

Photonic band gap crystals have many unique features. Band gaps can exist only in the directions of dielectric periodicity because scattering occurs along that direction. For a complete 3-D frequency gap, electromagnetic modes are totally suppressed inside the gap region, regardless the polarization. The structures then behave like ideal reflectors in all the directions. Similar to impurity doping of semiconductor crystals, localized EM modes (evanescent modes) can be created in the band gap region of PBG structures by disturbing the periodicity of the dielectric structures [4]. By adding extra dielectric materials to PBG crystals, a donor-like defect is introduced near the higher band edge, while removing some of the

material gives rise to a acceptor-like defect mode near the lower band edge. Likewise, surface modes are generated by the termination of dielectric periodic structures as well.

Another important feature of PBG crystals is that their band gap characteristics are scaleable to any length scales, ranging from microwaves to optical frequencies and beyond. Note that in semiconductor systems, the length scale is usually set by Bohr radius. As shown in equation (4), if the length scales of PBG structure are changed by a factor s ($r' = sr$ and $\nabla' = \nabla/s$), the wave equation for $\vec{H}(\vec{r})$ can be rewritten as

$$s\nabla' \times \left(\frac{1}{\varepsilon(\vec{r}'/s)} s\nabla' \times \vec{H}(\frac{\vec{r}'}{s}) \right) = \left(\frac{\omega}{c} \right)^2 \vec{H}(\frac{\vec{r}'}{s}) \tag{4}$$

or

$$\nabla' \times \left(\frac{1}{\varepsilon'(\vec{r}')} \nabla' \times \vec{H}(\frac{\vec{r}'}{s}) \right) = \left(\frac{\omega}{sc} \right)^2 \vec{H}(\frac{\vec{r}'}{s}) \tag{5}$$

with $\varepsilon(\vec{r}'/s) = \varepsilon'(\vec{r}')$. Therefore, the wave equation has a new eigenvalue of $(\omega/sc)^2$ for the eigen mode $\vec{H}'(\vec{r}') = \vec{H}(\vec{r}'/s)$ and frequency is simply scaled down by a factor of s.

Similar scaling effects have been observed if the dielectric constants of the structure are changed to $\varepsilon'(\vec{r}) = \varepsilon(\vec{r})/s^2$. The eigenequation then can be expressed as

$$\nabla \times \left(\frac{1}{s^2 \varepsilon'(\vec{r})} \nabla \times \vec{H}(\vec{r}) \right) = \left(\frac{\omega}{c} \right)^2 \vec{H}(\vec{r}) \tag{6}$$

or

$$\nabla \times \left(\frac{1}{\varepsilon'(\vec{r})} \nabla \times \vec{H}(\vec{r}) \right) = \left(\frac{s\omega}{c} \right)^2 \vec{H}(\vec{r}). \tag{7}$$

In this case, scaling down the dielectric materials of the whole system by a factor s^2 results in scaling up frequency of the new system by a factor s (i.e. frequency scale as 1/n.) The behavior of band gap characteristics has not been changed, as along as the dielectric constant ratio between materials is fixed.

I.3. Applications of Photonic Band Gap Crystals

The novel properties of photonic band gap structures have led to many potential applications over a wide frequency range. For example, PBG structures can be used to control optical properties in optoelectronic devices by overlapping the electronic band edges of the devices and the frequency gap of PBG structures. In the physical geometry, the active region of the device is surrounded with PBG materials as an optical cavity. Since the density of electromagnetic modes is very low inside the band gap region, the overall spontaneous emission for photons is then significantly reduced in the gap, creating higher efficiency light emitters such as ultra-low threshold semiconductor lasers [1] and single-mode light emitting diodes [5]. Depending on the application, PBG structures can also be employed to enhance the spontaneous emission rates at frequencies near the photonic band edges [6] or suppress the emission in the gap.

Other applications utilize the properties of high reflectivity and defect modes inside the gaps. PBG crystals are useful as dielectric mirrors in optical devices. In comparison with the traditional epitaxially grown mirrors that require many quarter wavelength-thick layers due to the small refractive index contrast in materials, three-dimensional PBG mirrors can provide higher reflectivity with fewer layers. Furthermore, with the mirror-like behavior, PBG crystals can be used to construct high-Q resonators or cavities and low-loss waveguides [4, 7] in many frequency regions. The effects of using PBG materials are more pronounced in the optical or infrared wavelength regimes, where metallic mirrors or waveguides are very lossy and

dielectric materials usually suffer from poor optical confinements as the light is transmitted around the tight corners such as in optical fibers [8]. In addition to their abilities to reflect, trap, and transport the EM waves, the potential applications of PBGs have recently been extended to nonlinear optical devices. The discovery of more applications can be expected in the future.

Many of the aforementioned applications rely on three-dimensional PBG crystals to provide better confinement and EM modes suppression in all directions for any polarization, particularly for $\lambda = 1.5$ μm in telecommunications. However, 3-D PBG applications have been realized only in microwave and millimeter wave frequency ranges, including efficient antennas [9] and high-Q cavities. Because of the difficulties in fabricating 3-D interlinked periodic structures with feature sizes 10 times smaller than the wavelength interested (for example, 0.1-μm feature sizes for PBG crystals at 1 μm), practical 3-D crystals with good performance for device applications are not available yet in optical or in near-infrared regions.

I.4. Statement of Purpose

To provide an alternative fabrication method for 3-D PBG crystals operating in infrared and optical wavelength regime, we have developed a process to construct them in a layer-by-layer fashion. This method uses sequential steps of wafer fusion bonding, selective substrate removal, and pattern etching in compound semiconductors to further scale down earlier works. The design issues of layer-by-layer PBG crystals and the choice of materials based on their transparent characteristics (negligible absorption loss) and high refractive indices in certain frequency range are discussed briefly. We have chosen semi-insulating GaAs epitaxial layers as PBG materials, which are suitable for PBG crystals with stop bands in mid- and near-infrared regions.

In our method, wafer fusion bonding techniques are used for stacking up the thin PBG layers. Comparisons between fusion bonding and different bonding methods are discussed to point out the advantages in using these techniques. Fusion bonding process for III-V compounds was then presented in detail. In our work, a thin (Ga,In)As "bonding" layer is incorporated to improve the bonding strength between GaAs wafers. The indium-based alloy material is chosen because of its high surface mobility, which results in significant amount of mass transport at elevated temperatures compared to Ga atoms. The key step of building up the PBG crystals relies on successful wafer bonding to stack up the layers smoothly and uniformly. We have investigated the characteristics of (Ga,In)As-based fusion bonded samples by varying bonding conditions and In content in (Ga,In)As alloys. Optimum bonding conditions are determined by analyzing bonded interfaces and surfaces, as well as optical measurements for the application of PBG crystals.

In addition, we report the process steps for fabricating of 3-D PBG crystals operating around 10 μm. Multi-layered periodic structures with 1-μm feature sizes are demonstrated. To study the effects of stacking up and patterning the PBG layers on their optical properties, transmission measurements after each process step are presented for further analysis. Finally, suggestions for reducing absorption and scattering losses from interfaces and etch patterns are described. With the further improvement of bonded interfaces, wafer bonding and micromachining techniques provide a promising way to realize photonic band gap crystals in mid-IR range.

II. LITERATURE REVIEW

II.1. Geometries of 3-D Photonic Band Gap Crystals

Photonic band gap crystals are multi-dimensional periodic dielectric structures which exhibit forbidden frequency ranges or gaps in the transmission spectrum. The existence of complete band gaps depends on lattice symmetry, direction of periodicity, ratio of the refractive indices between two materials in the structure, and filling factor. It was first predicted by Ho, Chan, and Soukoulis [10, 11] at Iowa State University that a 3-D periodic crystal with diamond or diamond-like lattice symmetry would have a full band gap.

It was found from theoretical calculations that these structures could show complete band gaps either with dielectric spheres placed at the diamond lattice sites or air spheres embedded in a high dielectric material as long as the diameters of the spheres were appropriately chosen and the refractive index contrasts were greater than 2 [10]. This threshold can be explained with the fact that significant scattering effects occur only when the variation of dielectrics is large enough. The photonic band gaps become wider as the ratio of refractive indices increases.

Moreover, the size of band gap has been optimized with a gap/midgap ratio of ~0.3 by choosing the diameter of the air spheres to be 0.65 a, where a is the lattice constant. In this case, the air spheres overlap with each other to form connected regions for both air and dielectric materials. Therefore, this structure can be considered to have two interpenetrating diamond lattices [8]. Without the isolated spots for both regions, the diamond-like photonic band gap structure shows a higher gap to midgap ratio. It also implies that photonic band gap crystals can be created by connecting the sites of a diamond lattice by dielectric rods or tubes [12, 13].

Following these principles, several specific three-dimensional geometries have been discovered having complete frequency gaps in all the directions [12-14] along with the potential fabrication at optical wavelength scales. In this chapter, we review the most notable 3-D dielectric PBG crystals and the methods for fabrication them in different frequency ranges. The limitations and difficulties associated with each technique are also stated in the following sections.

II.2. Yablonvitch's Three Cylinder Structures

The first three-dimensional photonic band gap crystals were experimentally demonstrated by Yablonovitch et al. [12] at centimeter length scales with a full frequency gap from 10 to 13 GHz. The structure has a diamond-like lattice symmetry as shown in Figure 1 and was made mechanically by drilling 3 sets of cylindrical holes 35° off vertical into each

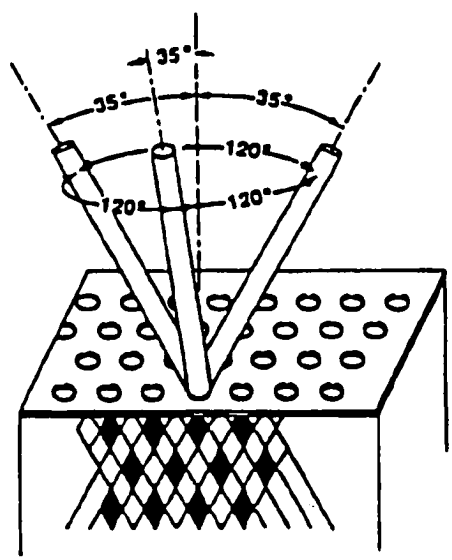

Figure 1. First three-dimensional dielectric photonic bandgap crystal. The diamond-like structure was fabricated by drilling holes at 35° from normal and 120° to each other [12].

triangle lattice site on top of the dielectric slab (stycast). Although this structure has shown good performance with attenuation of 10 dB per unit cell, it is difficult to scale down in size to infrared frequencies or even the millimeter wave frequencies.

Using microfabrication methods such as chemically assisted ion beam etching (CAIBE), a three-cylinder structure operating in near-infrared wavelength regime has been reported by Cheng *et al.* [15, 16]. Instead of conventional drilling, the periodic structure was formed by multiple angle etching processes through masking layers on a GaAs substrate surface. However, the overall vertical thickness of the periodic structure has been limited to just a few unit cells because the sizes of holes decreased significantly along the etch direction. Transmission characteristics inside the gap were very sensitive to this tapered-diameter effect, resulting in a rather small attenuation in the midgap and red-shifted band edges [16].

The limitation of sufficient depth from ion beam etching for a small dimension structure might be overcome by using deep x-ray lithography, followed by a molding step [17]. In this method, three tilted irradiations were used to transfer the mask patterns into a three-dimensional periodic structure in a thick radiation sensitive polymer (resist). This resist structure was then used as a mold, and the holes or empty spaces in the structure were filled with a high dielectric ceramic or preceramic materials to form a photonic band gap material. Using this technique, PBG structures in the infrared range were fabricated with a lattice constant of 85 μm and midgap frequency of 80 cm^{-1}.

II.3. Layer-by-Layer PBG Structures

Our group at Iowa State University has developed a new layer-by-layer structure [13], which exhibits a complete three-dimensional photonic band gap. As shown in the schematic diagram (Figure 2) of this structure, each PBG layer consists of a set of parallel dielectric rods. The geometry is arranged such that the rods between neighboring layers are rotated by 90° and

the parallel rods between second neighboring layers are shifted by half the repeat distance. This multi-connected 3-D periodic structure has a face centered tetragonal (FCT) symmetry with lattice repeat distance of 4 layers. In a number of experiments, this structure has been proven to be much easier to fabricate in smaller sizes and exhibit higher attenuation per unit cell compared to Yablonvitch's structure.

The layer-by-layer structure was initially built at microwave frequencies by mechanically stacking up layers of round alumina rods ($\varepsilon_r = 9.61$). It exhibited a complete three-dimensional gap between 12-14 GHz with an attenuation of ~16 dB per unit cell (4 layers). Transmission measurements were in good agreement with theoretical calculations. Subsequently, using standard silicon micromachining techniques — anisotropic etching of (110) wafers in KOH — and a simple mechanical stacking method, the layer-by-layer PBG crystals were scaled down from millimeter to submillimeter length scales with operating frequencies from 100 GHz up to 500 GHz, corresponding to $\lambda = 600$ μm [18-20]. Using

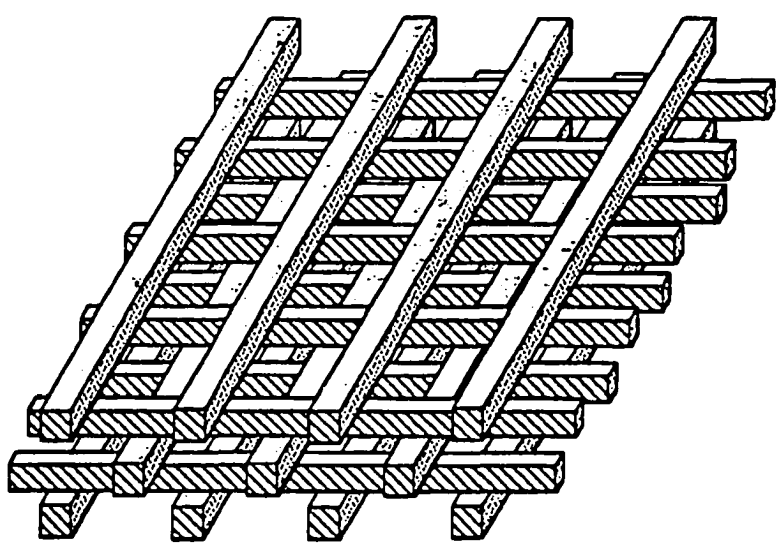

Figure 2. Layer-by-layer structure developed by Iowa State University's group [13].

these crystals, PBG applications have been reported in the area of antennas, resonators, and cavities in microwave and millimeter waves.

Recently, layer-by-layer PBGs with band gaps near 4 THz ($\lambda = 75$ μm) were fabricated using laser rapid prototyping [21] by means of laser-induced direct-write deposition from the gas phase. In this method, the layer of parallel aluminum oxide rods with 40-μm diameters was grown vertically on a silicon substrate by the technique of laser chemical vapor deposition (LCVD). The adjacent layer was then grown perpendicularly to the previous layer and connected together during the growth. Although this method has the advantage of being an additive process, as opposed to normal semiconductor etching methods, which are subtractive, and might be convenient for the defect structures, the achievable minimum rod diameters are ultimately limited by the focused spot sizes of laser beams.

More recently, Lin *et al.* [22] at Sandia National Laboratories have reported the fabrication of layer-by-layer crystals at $\lambda = 12$ μm. The structure was built by precise stacking and planarizing of multiple layers of poly-silicon. In each PBG layer, a poly-Si layer was deposited over a stripe patterned SiO_2. This overlayer was then planarized by chemical mechanical polishing (CMP) process. After repeating the processes and building up several layers, the whole structure was etched in a diluted HF solution to clean up SiO_2 material. With a large refractive index constrast of ~3.6 from the structure, gap to midgap frequency ratio of 35% has been achieved in the stacking direction, with attenuation of ~12 dB per unit cell.

II.4. Different Layered Structures

A different PBG layered structure, which might be fabricated at submicron length scales was proposed by Fan *et al.* at MIT [14]. The fabrication process of this structure begins with depositing of a layer of high index material and etching parallel grooves into it. The grooves are then filled with low dielectric material. Similar process steps are followed for the

next layer except that the grooves are shifted by half repeat distance. After building up multiple units (2 layers) vertically, an array of long cylindrical air holes is etched through the top surface perpendicular to the layers. The overall structure has the symmetry of body centered orthorhombic and can be constructed with common materials used in semiconductor processes. However, due to the difficulties in fabrication of this 3-D complex structure at submicron-length scales, further results have not been published yet.

II.5. Opal-Like Structures

The aforementioned three-cylinder and layer-by-layer PBG crystals are all artificially engineered periodic dielectric structures. Recently, the use of opal structures as 3-D PBG crystals has been proposed [23]. Natural opals or synthetic opals consist of SiO_2 spheres in 3-D face-centered-cubic (FCC) arrangements with diameters, D = 150 nm - 450 nm. Inside the material, the opal void lattices act as the scattering centers for a 3-D grating to generate stop bands in the visible range. However, owing to the small silica-air refractive indices contrast (1.45:1) and the FCC symmetry, the bare opal does not posses a complete band gap. This was improved by coating the voids inside the opal with high index materials such as InP using chemical vapor deposition technique. Even in that case, a high attenuation band gap has not been achieved because the refractive index contrast is still small, ~2.4.

III. DESIGN AND MATERIAL CONSIDERATIONS

III.1. Band Structures

The 3-D layer-by-layer photonic band gap crystals designed by the Iowa State group have been used to show scaleability over a wide frequency range. Contrary to the three-cylinder structures, precise control of dimensions in each PBG layer is achievable in fabrication process because of the layered design. Figure 3 shows the calculated band structure of the layer-by-layer PBG crystal as a function of wavevector [13]. Photonic band gap calculations were done using vector wave equations in a plane-wave expansion method [10]. The use of vector-wave band theory is necessary, due to the polarization coupling of EM waves in the PBG crystals.

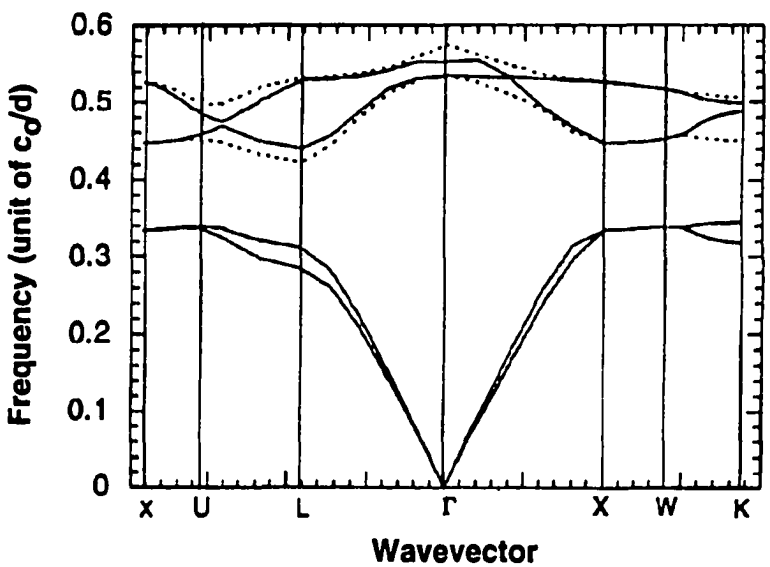

Figure 3. Photonic band structure of this FCT lattice for the six lowest bands. The dielectric contrast of materials is 12.96. Filling ratio of the dielectric material = 0.3 [13].

III.2. PBG Design Considerations

The layer-by-layer PBG crystal exhibits a complete gap in all directions over a wide range of structural parameters. The center-of-gap frequency, υ_{midgap}, and width of the gap, $\Delta\upsilon$, are determined by the geometry, structural dimensions (seen in Figure 4), and refractive index contrast, n_c, between two materials. Midgap frequency and wavelength are given by

$$\upsilon_{midgap} = \gamma\,(c_0/a) \quad \text{or} \quad \lambda_{midgap} = a/\gamma \tag{8}$$

and

$$\gamma = \gamma(c/a,\ f,\ n_c), \tag{9}$$

where γ is the normalized frequency and can be extracted from band gap calculations. In the

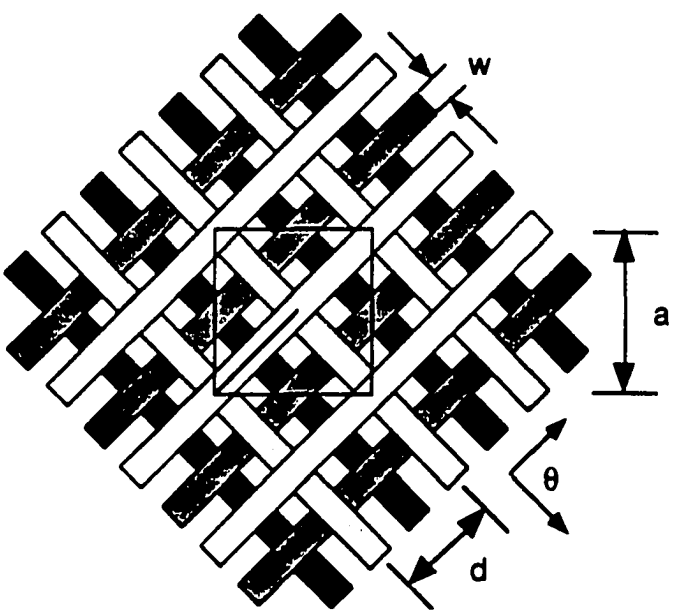

Figure 4. Schematic diagram of a 4-layer PBG crystal, with a = 1.414 d and θ = 90°.

above equations (8) and (9), c_0 = speed of light, a = lattice constant in the x-y plane, c = lattice constant or repeat distance in the stacking direction, w = width of the dielectric rod (square cross section), d = repeat distance of the dielectric rods in x-y direction, and f = w/d is the filling ratio of the dielectric material. This layer-by-layer PBG structure can be distorted by varying θ over a range from 90° to 60° [24], while still maintaining a sizable full band gap. For an orthogonal structure as shown in Figure 3, a = 1.414 d and θ = 90°.

The PBG structure can have a full gap with refractive index contrast as low as 1.9. The gap/midgap ratio increases with increasing n_c, while the midgap frequency decreases with n_c. Figure 5 shows the gap/midgap frequency ratio as a function of filling ratio with various c/a ratios for rectangular rods structures. It is clear that gap/midgap ratio drops down quickly for c/a > 1.414 and c/a < 0.57, and it peaks at 0.19 with f = 0.27 and c/a = 0.86 for n = 3.60.

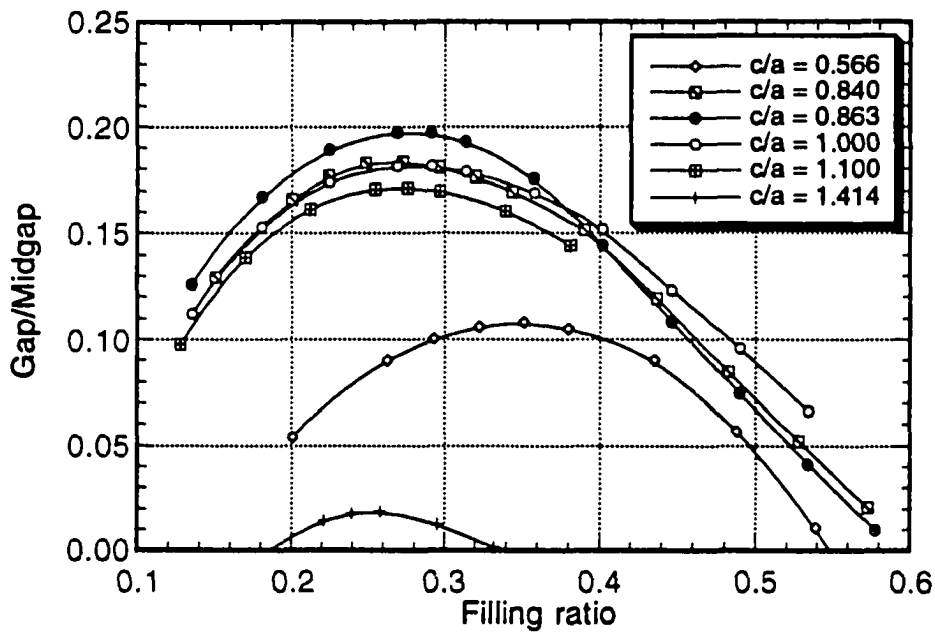

Figure 5. Gap/midgap ratio as a function of filling ratio for various c/a values [13].

Variations of the filling ratio and c/a ratio from optimized values do not shift the target gap width and midgap frequency significantly, which gives some flexibility in designing and fabricating the structure. It is especially crucial for the PBG crystal with submicron sizes because dimensional variation and non-uniformity in fabrication processes could be an issue.

The normalized frequency γ (in units of c_0/a) decreases with increasing filling ratio, while it increases with c/a values for a fixed filling ratio, as presented in Figure 6. This can be explained qualitatively using the effective dielectric constant of the whole material, $\varepsilon_{eff} \approx \varepsilon_{high} f + \varepsilon_{low} (1-f)$, since midgap frequency is proportional to $(\varepsilon_{eff})^{-0.5}$. Furthermore, the cross-sectional configuration is not critical in determining the existence of a gap. For a dielectric cylinder with a pinched cross section (the width at the midpoint is narrower), which is the

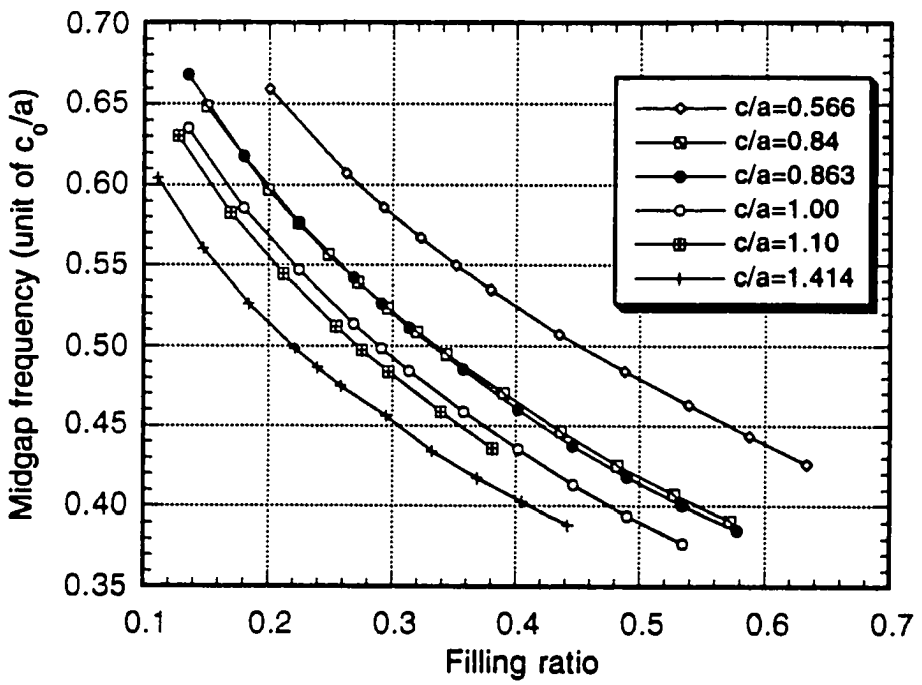

Figure 6. Midgap frequency as a function of filling ratio for various c/a ratios and n = 3.60 [25].

common etch profile for III-V semiconductors in wet chemical etching, a sizable gap is still obtainable, even though the pinched structure does have a slightly reduced gap-to-midgap frequency ratio.

Another structural variation is that the air cylinders in the layer-by-layer structure can be disconnected from each other. For example, in the underetched air cylinder structure (see the inset of Figure 7), the connected dielectric layer, with a width of h, can be as thick as 5% of the target layer thickness, t. In this case, the Gap/midgap ratio or gap width only reduces less than 1/3 as shown in Figure 7 [26]. This adds another degree of freedom for designing 3-D PBG structures.

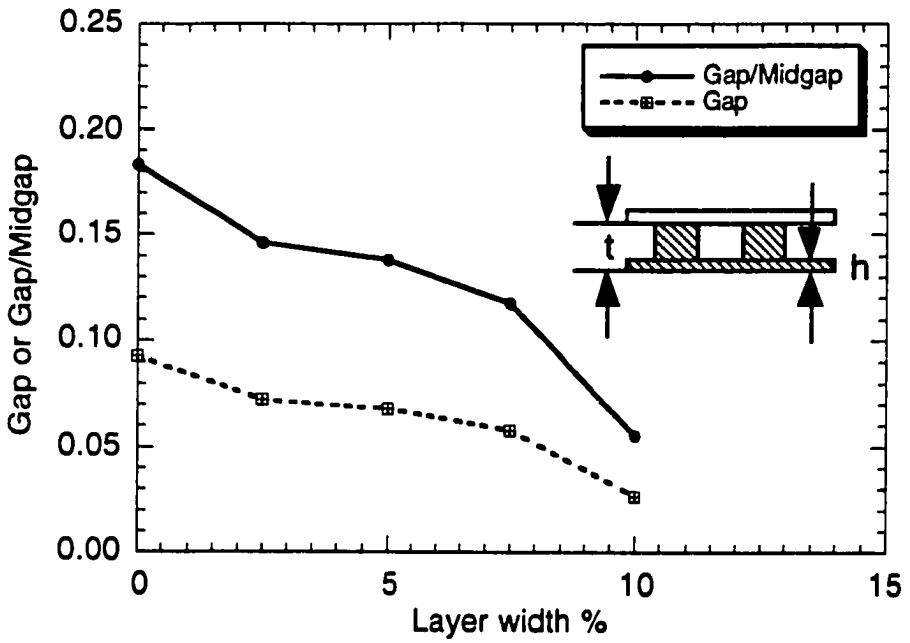

Figure 7. Calculated gap or gap/midgap as a function of layer width % for an underetched air cylinder structure. The PBG structure consists of rectangular rods and n = 3.6 [26].

III.3. PBG Material Considerations

The photonic band gap opens up as the refractive index contrast (n_{hig}/n_{low}) of the materials becomes larger than ~2.0 and the size of the gap increases with increasing ratio of (n_{hig}/n_{low}). The transmission and reflection properties of PBG crystals are strongly influenced by the absorption of the materials. Therefore, the choice of PBG material should meet two major criteria — high dielectric constant and low optical absorption. Among various dielectrics, the common insulators used in industry such as SiO_2, Si_3N_4 [27], MgO, $BaTiO_3$, and polyethylene $(C_2H_4)_n$ [28] have shown good transmission for near-visible light, but have low values of n. In contrast, most semiconductor materials have the advantage of high refractive index of ~3.6 in optical regime. Table 1 lists the optical properties of various semiconductors and insulators that could be used as PBG materials. The suitable wavelength ranges (in units of μm) for semiconductors shown in the table are limited by the band-to-band absorption edges (lower bound) and phonon absorption (upper bound) in the far-infrared range.

As shown in the table, aluminum oxide (Al_2O_3) is a good PBG material for microwave and millimeter wave applications but has a strong absorption in mid-IR range. Although II-VI materials (CdTe and CdSe) have extended low absorption ranges, their refractive indices are not the highest in semiconductors. In the past, high resistivity Si has been used to make PBGs successfully at millimeter wave and terahertz frequencies. However, as stated in the previous chapter, Si thin films for PBG layers in mid-IR or optical regions are much less accessible, compared to III-V epitaxial materials.

From the above discussion, it is clear that III-V semiconductors have several advantages. We have chosen semi-insulating (SI) GaAs epitaxial layers as PBG materials based on their availability from our facility and broad transparent transmission characteristics

Table 1. List of optical properties for various semiconductors and dielectric materials [27, 28].

Material	Refractive index	Low absorption range (μm)	Reference
Si	3.6-3.4	1.0-16	[27]
Ge	4.2-4.7	1.6-22	[27]
GaAs	3.6-3.2	0.9-18	[27]
AlAs	3.4-2.7	0.5-14	[28]
InAs	3.6-3.3	3.7-22	[27]
GaSb	4.1-3.7	1.6-29	[28]
AlSb	3.7-2.8	0.7-25	[28]
InSb	4.0-3.9	8.0-20	[27]
GaP	3.5-3.0	0.5-10	[28]
InP	3.4-3.0	0.9-14	[27]
CdTe	2.9-2.5	0.8-30	[27]
PbSe	4.9-4.8	5.0-10	[28]
CdSe	2.8-2.3	0.7-25	[28]
Al_2O_3	3.2-3.3	100-1000	[28]

(negligible absorption loss) together with their high refractive index of ~3.3 between 1 μm and 18 μm. Figure 8 shows the measured transmission characteristics of a 500 μm-thick (SI) GaAs substrate as a function of wavenumber ($1/\lambda$) in far- and mid-infrared regions, respectively. The interference fringes from the rapid phase change do not show in the measured transmission curve because of the averaging effect from instrument. However, the transmission intensity is consistent with calculations from reflection, $(n-1/n+1)^2$ and transmission, $(2n/n+1)^2$ of the dielectric material of n. The small peaks and strong absorption bands in far-IR region are due to phonon and multi-phonon absorption processes, which arise from the bond bending and bond stretching vibrations of GaAs. Hence, the material is good for PBG crystals with stop bands in mid- or near-infrared regions.

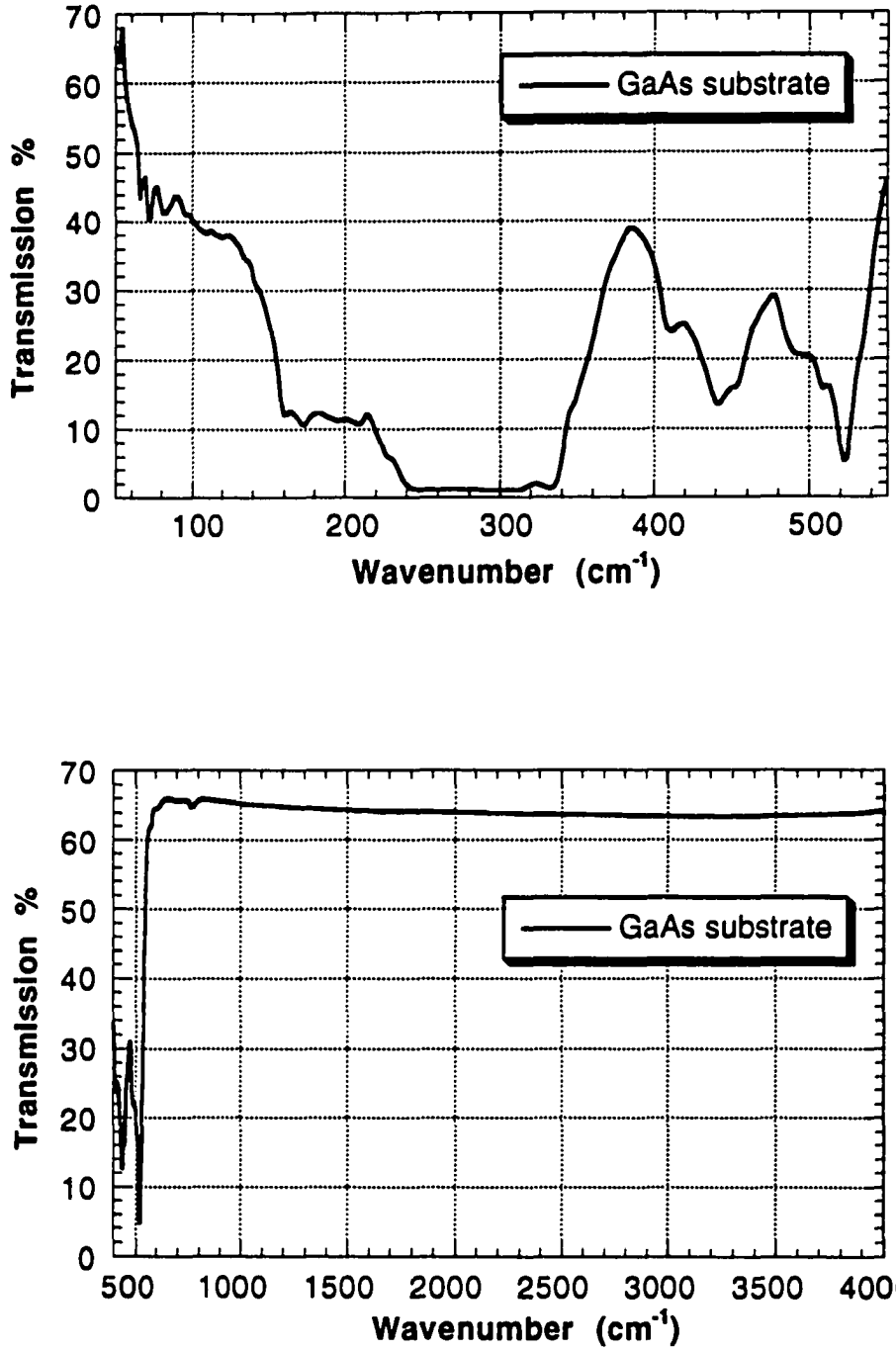

Figure 8. Transmission spectra of a 500-μm thick (SI) GaAs substrates in far- (50-600 cm^{-1}) and mid-IR (400-4000 cm^{-1}) regions.

IV. WAFER FUSION BONDING

IV.1. Thin Film Transfer

For three-dimensional layer-by-layer PBG crystals operating below 1 THz, micromachining techniques take advantage of simultaneous processing of Si full wafers and mechanical assembly of patterned wafers, as reviewed in the previous chapter [18-20, 29]. The relatively small air gaps or glue between the stacked layers did not degrade the transmission properties, because scattering and diffraction losses are not significant in this long wavelength range. To further scale down the structure in size to the mid-infrared frequency range or higher, the thickness of each layer must be reduced to micron-length scales. Stacking becomes an essential step to build up PBG thin layers in the modified micromachining process, and it relies on thin film transfer techniques to achieve the required interface conditions between adjacent layers.

Thin film transfer methods have been used to integrate different semiconductor materials to optimize device performance for various applications, as well as to create new layered structures. In general, this method can be divided into wafer bonding and thin film bonding techniques. In the latter, a thin film is separated from its substrate before it is bonded to a target substrate. In wafer bonding, the film is separated from its substrate after the bonding. Therefore, it has an advantage of easy handling over the thin film bonding during fabrication processes. In this section, different bonding approaches, including silicon direct bonding, epitaxial lift-off, metal bonding, and wafer fusion bonding are reviewed. We also discuss their potential uses and drawbacks in constructing three-dimensional layer-by-layer PBG crystals.

IV.2. Bonding Techniques

IV.2.1. Silicon direct bonding

Silicon direct bonding (SDB) is the most widely studied and used wafer bonding technique. Two silicon wafers are bonded together with either bare silicon surfaces or oxidized surfaces right after a surface chemical treatment. Depending on surface conditions, the two wafers are held together at room temperature either by bonding between Si-OH groups (hydrophilic bonding) [30, 31] or by short-range van der Waals forces (hydrophobic bonding) [32, 33]. Subsequent heating at higher temperatures in N_2/O_2 ambient increases the bonding strength between the wafers without any external pressure applied. In general, annealing temperatures as high as 1000-1200 °C for 1-2 hours are necessary for hydrophilic bonded wafers to remove any bubbles or voids resulting from water evaporation during the heating process. One of the applications of SDB is to bond a bare Si wafer to an oxidized silicon wafer. Then the substrate is thinned down to a specific thickness by mechanical lapping and/or chemical etching, producing a Si on insulator (SOI) substrate. Using similar methods, a thin Si layer can also be transferred to another Si substrate. However, due to the lack of available Si thin layers and the extremely high temperature cycle, SDB is probably not suitable for complex PBG structures.

IV.2.2. Epitaxial lift-off (ELO) bonding

In this technique, III-V semiconductor thin films are bonded onto arbitrary materials, including semiconductors and insulators (Si, III-V's, SiO_2, $LiNbO_3$), by van der Waals bonding due to the intermolecular attractive forces [34, 35]. The desired thin film is first separated from its substrate in the epitaxial lift-off (ELO) process with a thick layer of Apiezon W wax applied on top as a mechanical support for handling. In ELO, the wafer is immersed in a wet chemical solution and the transfer thin film is released from the substrate using the highly

selective etching (in lateral direction) of an ultra-thin sacrificial layer. For the bonding process, the thin film is rinsed in de-ionized water and placed on a substrate with pressure applied on top. Bonding takes places as the water dries and the surface tension of water pulls the film down to the substrate.

ELO-bonding has the advantage of being a room temperature process, but process reliability is not very high with the interfacial layers. Also cross-sectional transmission electron microscopy studies [34] often show that a hydrated oxide layer (20-140 Å) forms at bonding interface, which could cause scattering losses for optical devices and degradation of electrical properties. Another drawback of ELO-bonding is that the quality of bonded thin films decreases in the pro-bonding high temperature process.

IV.2.3. Metal bonding

In the past, interfacial metal layer with Pd have been applied to epitaxial lift-off (ELO) process to improve the reproducibility [35]. In the bonding process, low temperatures (< 200 °C) can be used because of the high surface diffusivity of Pd, which produces effective mass transport even at room temperatures. Furthermore, to integrate semiconductor devices to different substrate materials, metal thin films have been used to bond InP detectors to GaAs substrates [36], AlGaAs emitters to Si substrates with Au at ~430 °C [37], and GaAs surface-normal modulators to Si wafers with In [38]. However, metal layers are usually lossy at high frequencies and might not be suitable for photonic band gap crystals in the optical regime.

IV.2.4. Wafer fusion bonding

Wafer fusion bonding of III-V semiconductors is similar to Si wafer bonding. The bonding process relies on high annealing temperatures and uniform pressures to ensure robust bonding at the interface. The applied pressures reduce the gaps between two contacting surfaces, while high temperatures provide sufficient mass transport to fill in the gaps and

cavities. Because of the covalent bonding of the atoms from two materials, fusion bonded interfaces are very stable. This technique was first presented by Liau and coworkers in 1984 [39]. Later, Liau demonstrated a p-n junction by fusing InP to InP substrates and InP to GaAs substrate at 830 °C for 2 hours [40]. Lo *et al.* [41] used similar fusion technique, bonding by atomic rearrangement (BAR), to bond InP-based laser on GaAs substrates at lower temperatures of 650 °C for shorter time (30 min.) over an area of 2 cm^2.

Wafer fusion has been applied to integrate different III-V semiconductors to achieve the desired device performance by utilizing a thin InP as bonding layer. Wide range of applications has been reported such as fusing of GaAs/AlAs DBRs to InP-based laser structure [42, 43] and InGaAs photodetector [44], AlGaInP LEDs to transparent GaP substrates [45]. In addition, wafer fusion has been used to stack GaAs layers together [46], as well as InGaP [47] together for second-harmonic generation in waveguides. The III-V photonic devices have also been integrated to Si for InGaAs/GaAs laser structures [48] and InGaAs photodetectors at 650 °C [49]. Recently, InSb thin layers have been reported to grow on GaAs compliant substrates that contained 30 Å twist-fusion bonded GaAs layers [50].

IV.3. Wafer Fusion Bonding for PBG Crystals

As reviewed in the previous section, wafer fusion is the best bonding technique for GaAs materials for stacking up multiple thin layers, although it requires high temperatures and pressures. In this section, details of GaAs-based fusion bonding process and material preparation are presented. For fusion bonding experiments, our initial work involved bonding between GaAs epitaxial layers and GaAs substrates. However, experimental results showed that In atoms exhibit higher mobility compared to Ga atoms [48], which resulted in improved bonding interfaces. In our experiments, we used a thin (Ga,In)As "bonding layer" that was grown on top of the GaAs transfer layer to increase the bonding strength. The effects of

varying bonding conditions and In content in (Ga,In)As layers on fused interfaces were studied.

For purpose of comparison, we also conducted bonding experiments in which a thin layer of pure indium metal was used as a "bonding agent." The In layer was deposited by E-beam evaporation on the surface of GaAs transfer layer of a target substrate prior to bonding. Similar bonding conditions were applied to (Ga,In)As-based bonding as in the wafer fusion experiments. Furthermore, the bonded samples were characterized for mechanical and optical properties to determine the optimum bonding conditions for constructing the multi-layered PBG structures.

IV.3.1. General process for wafer fusion bonding

For GaAs wafer fusion experiments, 7 mm x 7 mm double-side polished semi-insulating (SI) GaAs (100) target substrates and MBE-grown transfer wafers were used as bonding samples. The transfer wafers consisted of a GaAs substrate, followed by a 1-μm thick $Al_{0.8}Ga_{0.2}As$ (abbreviated as AlGaAs) etch-stop layer, a 1-3 μm thick GaAs transfer layer, and a thin In-based "bonding layer" ($In_xGa_{1-x}As$ layer). For the etch-stop layer, $Al_{0.8}Ga_{0.2}As$ was used instead of AlAs because AlAs is oxidized easily when exposed to water. This oxidized material changed the selectivity in etchant and was difficult to remove later. The typical fusion process for GaAs-based wafers is shown in Figure 9.

Before starting the wafer bonding process, the transfer substrates were first thinned to 150-200 μm by mechanical lapping. The bonding surfaces were then cleaned with acetone and methanol to reduce particulate and organic contamination, and etched in a buffered HF solution to remove any native oxides before being placed in face-to-face contact. The stacked wafers were placed inside a graphite holder (described in Appendix A) and put into an annealing furnace tube for fusion bonding. The temperatures ranged from 600-700 °C for times ranging

from 20 min. to 7 hours in a flowing H_2 ambient. The wafers were pressed together in a jig that provided a uniform pressure of 300 g/cm^2 to help ensure robust bonding.

After the high-temperature bonding step, the GaAs transfer substrate was then selectively removed in a citric acid/hydrogen peroxide (4:1) solution and the AlGaAs etch-stop layer was etched away in a diluted hydrofluoric acid solution ($HF:H_2O = 1:10$), leaving the thin GaAs transfer layer. Because the bonded sample would be attacked by the selective etch, they were glued to glass slides and sidewalls of the samples were protected with photoresist in the etching process. Care should be taken to avoid the photoresist flowing over the edges.

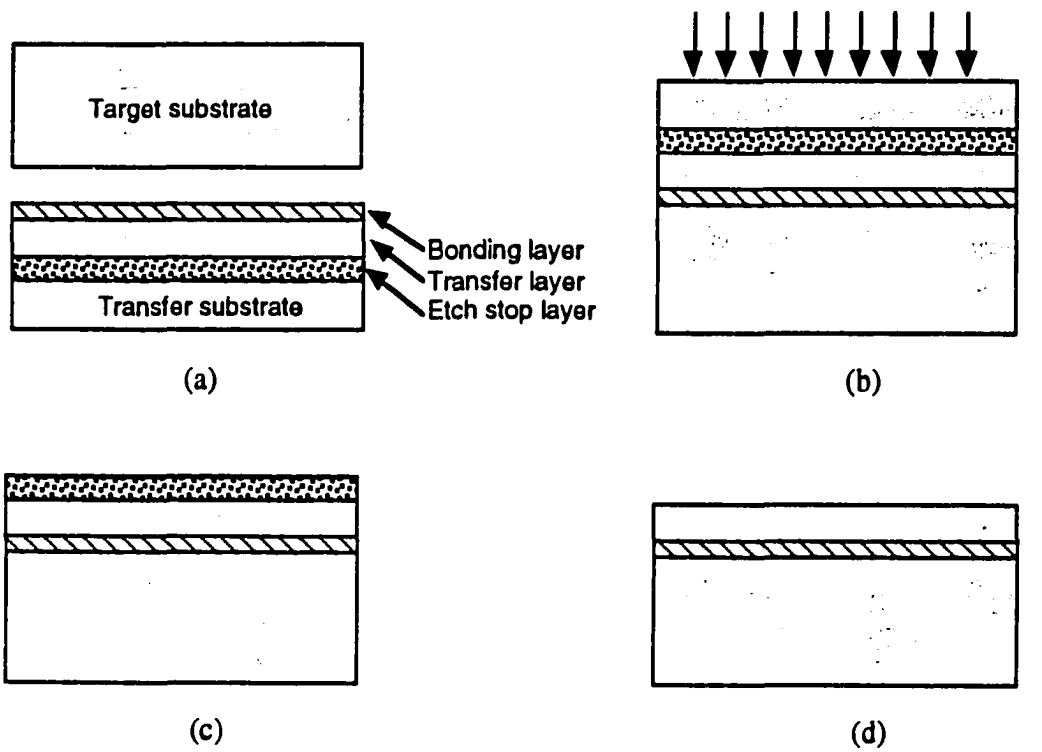

Figure 9. Wafer fusion bonding process: (a) Clean GaAs and transfer substrates; (b) Fuse wafers together at 650 °C; (c) Remove GaAs substrate; (d) Remove etch stop layer.

IV.3.2. Characterization methods of fusion bonding

After wafer fusion bonding and selective removal of the substrates and the etch-stop layers, the surfaces of GaAs transfer layers on the GaAs target substrates were examined under a Normarski microscope for surface flatness. The bonding interfaces were investigated by scanning electron microscope (SEM) and energy dispersive x-ray spectroscopy (EDS). Optical properties of bonding interfaces were characterized. The transmission characteristics of bonding interfaces in the stacking direction were measured with a Fourier transform infrared (FTIR) spectrometer (Nicolet model Magna IR 760) ranging from 400 cm^{-1} (25 μm) to 4000 cm^{-1} (2.5 μm) in mid-infrared range. The FTIR spectrometer had an unpolarized IR source, KBr beamsplitter, and KBr detector in mid-IR (A detailed discussion of the FTIR spectrometer and experimental setup are presented in Appendix B.) All the spectra were measured with 4 cm^{-1} resolution, 100 sample scans, and 4-mm aperture in front of samples. Prior to the measurements, the sample chamber of FTIR is purged with N_2 for at least 1 hour to remove the water vapor and carbon dioxide, which could cause prominent absorption bands in mid-IR frequency range. During the measurements, the N_2 purge was dropped down to 20 sccm to reduce the vibration of beamsplitter.

IV.4. Surface Characterization of Fusion Bonded Samples

Without the aid of intermediate thin bonding layers, fusion bonding did not take place between two polished GaAs surfaces, even though they had low surface roughness of 0.1-0.2 nm, as were measured by atomic force microscopy (AFM). We found the following conditions were needed to achieve smooth and uniform GaAs surface layers when using InAs-based bonding interfaces:

- Annealing temperature — The annealing temperatures needed to be 650 °C or higher. At temperatures less than 600 °C, the bonding samples did not stick

together at all. For annealing temperatures between 600 °C and 650 °C, the wafers were bonded but surfaces were not smooth across the whole area as shown in Figure 10(a).

- Annealing time — Annealing times also played a crucial role in the fusion process. We found the minimum annealing time to be 30 minutes. Less annealing time degraded bonding quality and also reduced the reliability of the process (see Figure 10(b) and 10(c)).
- Hydrogen flow — A flow of hydrogen was necessary in our fusion bonding process. We have found that fusion did not take place in a pure N_2 ambient. It has been suggested [41] that H_2 gas reacts with naive oxides at the bonding interfaces to form H_2O which is then carried out of the samples to ensure good bonding.
- Pressure — A weight of 300 g/cm^2 is sufficient to have robust bonding.
- In-based material — The InAs layer could be as thin as 500 Å. Without the InAs layer, GaAs wafers could not bond well at 650 °C and the process was not reliable. The much higher surface mobility of In atoms increased the mass transport effect which was essential for filling out the gap between two surfaces.

Multiple fusing steps have also been performed at 650 °C to successfully stack up several epilayers with smooth surfaces. The fused interfaces show strong mechanical strength to endure subsequent high temperature processes without cracking or peeling-off. Beside the bare GaAs wafer bonding, patterned surfaces have been bonded successfully under the same fusion conditions. The minimum feature sizes of the parallel bars could be as small as 1 μm with 1-μm depth, and we did not observed the gaps closing.

(a)

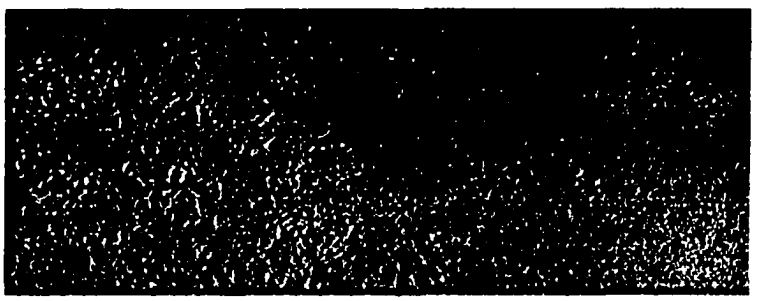

(b)

(c)

Figure 10. Comparison of bonded GaAs surfaces with different annealing temperatures and times. (a) 630 °C for 20 minutes (b) 650 °C for 20 minutes (c) 650 °C for 30 minutes.

IV.5. Optical Characterization of Bonded Samples

IV.5.1. Bonding of InAs/GaAs to GaAs substrates

As shown in section IV.4.1., smooth and uniform bonding surfaces of InAs/GaAs epilayers on GaAs substrates have been achieved at annealing temperatures of ~650 °C with pressures of 300 g/cm^2 in a H_2 ambient. More importantly, for realization of PBG crystals using this technique, we needed to investigate the optical properties of bonded interfaces. Numerous bonding experiments were conducted, and the final bonding samples which consisted of 1.0 μm of GaAs transfer films, 0.06 μm of InAs bonding layers, and 500 μm of polished (SI) GaAs substrates as presented in Figure 11 were characterized.

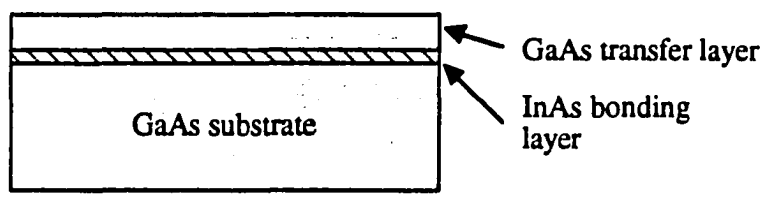

Figure 11. Fusion bonding sample with GaAs transfer layer, InAs layer, and GaAs substrate.

Figure 12 shows the measured transmission spectra (at normal incidence) of these fusion bonded flat samples with an annealing temperature of 650 °C for various lengths of annealing time. Below 600 cm^{-1}, the spectrum is dominated by multi-phonon absorption bands of the (SI) GaAs substrate in infrared frequency range as seen in the transmission spectra of GaAs in Figure 8. The interference patterns show up clearly across the spectrum range due to the GaAs transfer layer and the change of refractive index at GaAs/InAs interface. The separation of the interference fringes is related to the thickness of layer, L, with the relationship

$\Delta (1/\lambda) = 1/(2nL)$. The peak positions roughly match with predicted results, which were calculated using a transmission matrix method. For the bonding sample with annealing temperature at 650 °C for 5 hours, the overall transmission clearly drops from about 55% at 1700 cm^{-1} to 25% at 3200 cm^{-1}. Similar behavior is observed for each curve.

Robust bonding and smoothly bonded surfaces can be obtained for a wide range of bonding times. However, from the measurements the transmission intensities show strong dependence on the length of the heat treatment in the bonding process, especially at higher frequencies (2500-4000 cm^{-1}). The transmission peak intensity around 3000 cm^{-1} increases to 42% from 25% as the annealing time decreases from 5 hours to 30 minutes. The peak

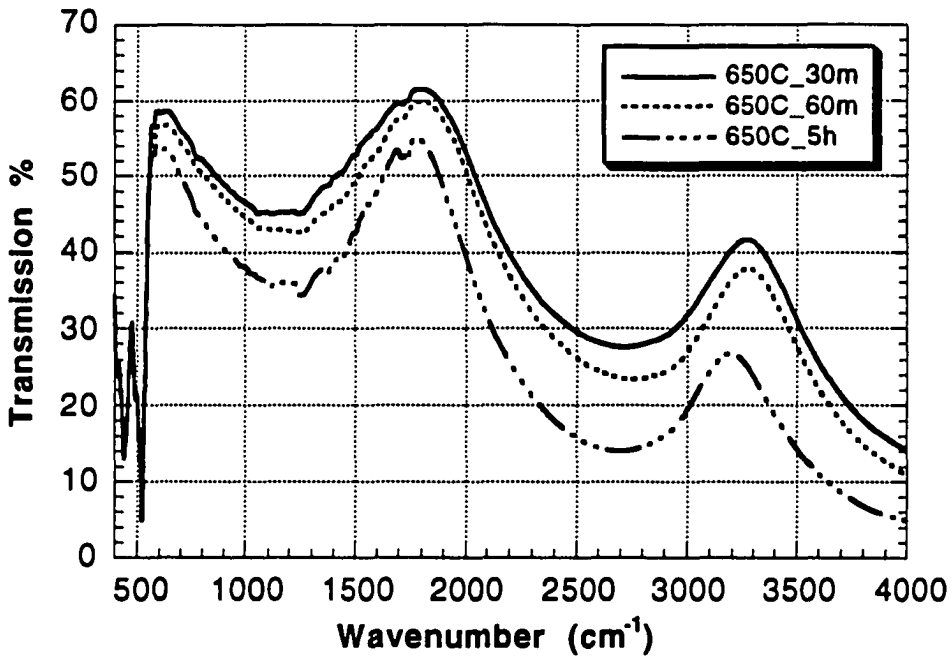

Figure 12. Measured transmission characteristics of fusion bonded samples at 650 °C for various annealing times with a thin InAs as "bonding" layer. Here GaAs transfer film is 1.0 μm, InAs bonding layer is 0.06 μm, and GaAs substrate is 500 μm.

positions have also shifted slightly to higher frequencies for shorter heat treatment.

Presumably, this is due to increased absorption at the bonding interfaces. Increase in absorption over the measurement range may be attributed by several factors: absorption in the InAs layer ($\kappa = \mathrm{Im}(n) \sim 0.14$ at 4000 cm^{-1}) [27], the absorption in pure In metal resulting from the decomposition of InAs material during the heating process, and the scattering at the nonuniform bonding interfaces. Therefore, by increasing the annealing time the bonding interlayer might become more lossy due to the material decomposition and due to an increase in the scattering effect.

IV.5.2. Bonding of In/GaAs to GaAs substrate

For purposes of comparison, we also conducted bonding experiments in which a layer of pure In metal was used as a "bonding agent." We used a 28 nm-thick In layer, which has the same amount of In as in the 60 nm-thick InAs used in the previous bonding. The same bonding conditions (anneal temperature of 650 °C, H_2 flow, and pressure of 300 g/cm^2) were applied to In-based bonding as in the InAs-based fusion bonding. To study the material properties of In thin film, a 28 nm-thick In was also deposited directly on GaAs substrate.

Figure 13 shows a comparison of transmission measurements of an In thin-film on a bare GaAs substrate. The absorption of In metal increases as the wavenumber increases. From measurements and $\alpha \left(=\frac{4\pi\kappa}{\lambda}\right)$, $\kappa = \mathrm{Im}(n)$ is roughly estimated to be 5.67 at 4000 cm^{-1}. The transmission spectra of the In metal bonded samples at normal incidence are shown in Figure 14. In contrast to the sharp decrease in transmission intensities at higher frequencies from InAs-based wafer bonding (Figure 12), a less pronounced decrease has been observed in In metal bonding. The optical losses for the In bonded samples seem mainly due to the absorption of In metal in mid IR range. They are in good agreement with the results shown in Figure 13. Moreover, the measured curves do not show strong dependence on annealing time. For increasing time from 30 minutes to 5 hours, the transmission drops less than 5%.

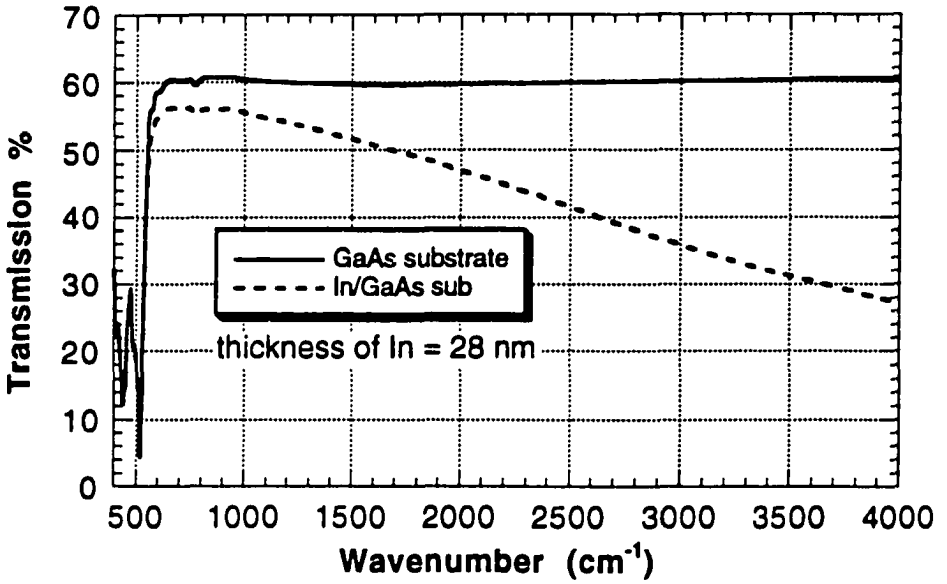

Figure 13. Transmission spectra of GaAs substrate and In metal on GaAs substrate.

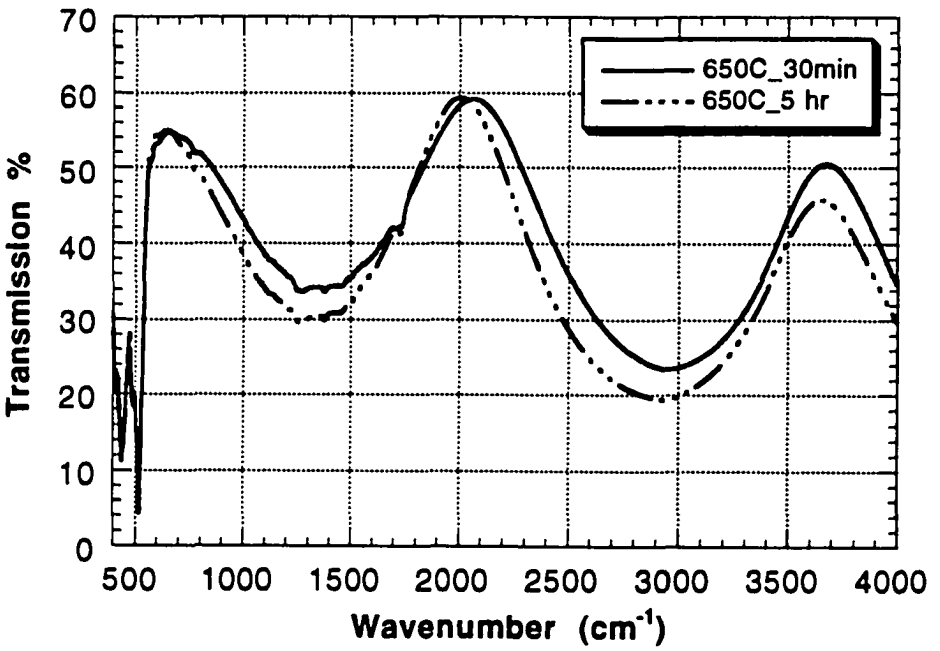

Figure 14. Measured transmission spectra of bonded samples at 650 °C with a thin In layer as "bonding" layer.

The peak positions have been moved to higher frequencies and the separation between two peaks increases from ~1500 to 1625 cm^{-1} compared to the previous results because of the slightly thinner GaAs layers used (~0.92 μm). Before indium metal deposition, the GaAs transfer layer was etched in a PAW solution (H_2O_2:NH_4OH:H_2O = 1:20:40) for 30 seconds to smooth out the surface.

The transmission characteristics suggest that, with reduced In layer thickness and associated absorption, In metal bonding could be an alternative method for fabrication of 3-D PBG crystals. However, we observed that decreasing the In metal thickness made the bonded surfaces less smooth and uniform. This might be related to the amount of indium needed to fill out the gaps.

IV.5.3. Bonding of (Ga,In)As/GaAs to GaAs substrate

To reduce the lattice constant mismatch between InAs and GaAs as well as material absorption, (Ga,In)As-based fusion bonding was studied by varying In content in the $In_xGa_{1-x}As$ bonding layer. In the bonding process, a 60-nm thick (Ga,In)As layer with x=0.67 replaced the InAs layer. For the same annealing temperature, 650 °C, smooth and uniform surfaces could not be achieved unless the annealing time was increased to ~7 hours. For robust bonding, a short time was used only if the annealing temperature was higher than 650 °C. Figure 15 shows the transmission measurements of bonded samples for two sets of bonding conditions. It is clear that decreasing In content plays an important role in improving the overall transmission properties. Compared to InAs bonding, good transmission is obtained for wavenumbers < 2000 cm^{-1}, and the peak intensity around 3000 cm^{-1} moves up significantly to 54% from 25%.

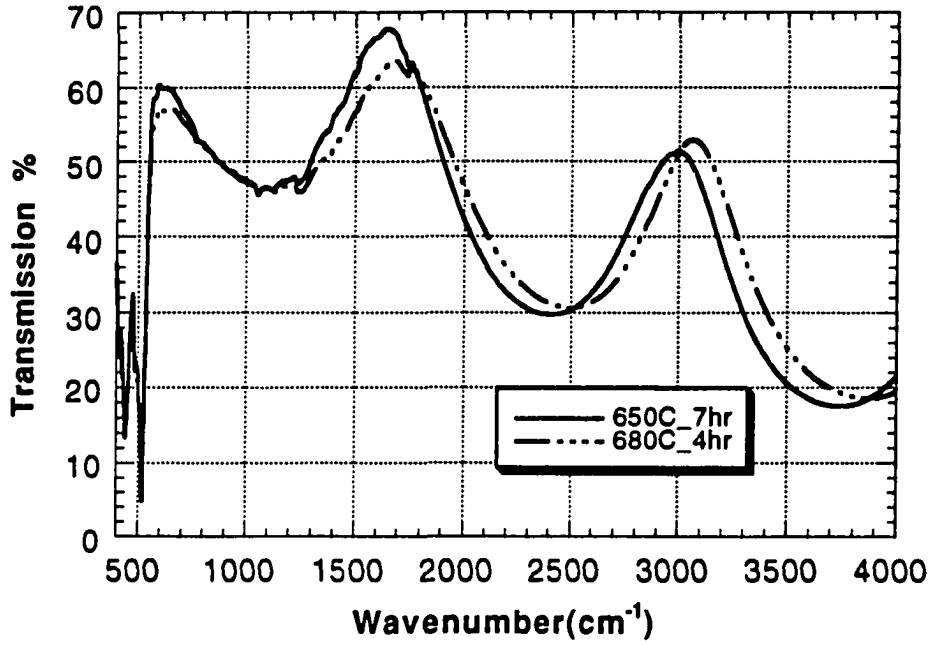

Figure 15. Measured transmission spectra of bonded samples at 650 °C with a thin (Ga,In)As layer as "bonding" layer.

IV.6. Analysis of Bonded Interfaces

The fusion bonded interfaces between (Ga,In)As/GaAs epilayers and GaAs substrates were also studied by SEM and energy dispersive x-ray spectroscopy (EDS). Analysis of the interfaces showed that a ~300 nm-thick layer with gaps formed between GaAs transfer layer and GaAs substrate. For InAs-based bonding, the number and size of air gaps seem to increase slightly as the annealing time increases, but the thickness of the interlayer remains about the same and does not show strong dependence on the annealing time and In content in the (Ga,In)As-based bonding. The composition of interlayers, as analyzed by EDS using line

scan technique and x-ray mapping, contained In, Ga, and As atoms inside the layer. In addition, EDS analysis shows that $In_xGa_{1-x}As$-based bonding (x=0.67) has a lower In/Ga ratio compared to the results obtained from the pure InAs bonding as expected. It was speculated that during the heat treatment, (In,Ga)As clusters or In metal particles were formed between GaAs materials. The origins of clusters could be related to the large lattice mismatch, 7.8% between GaAs and InAs layers, and the thermal induced stresses.

V. PHOTONIC BAND GAP CRYSTALS

V.1. Fabrication Process

The 3-D layer-by-layer PBG crystal (see in Figure 2) has a face-centered tetragonal (FCT) lattice symmetry, which can be formed by replacing the (110) chains with dielectric cylinders in a diamond structure. The structures were fabricated in a layer-by-layer fashion using alternating micromachining steps of wafer fusion bonding of GaAs-based semiconductors, selective substrate removal, and pattern etching.

The fabrication process began with preparing the bonding samples, a (SI) GaAs target substrate with a stripe pattern etched in the top surface, and MBE grown epilayers of AlGaAs, GaAs, and InAs (usually 500-600 Å) on the GaAs transfer substrate as shown in Figure 16(a). The array of parallel GaAs bars, covering an area of 4 mm x 4 mm, was defined by standard photolithography and reactive ion etching (RIE). The transfer substrate was then bonded to the patterned substrate using GaAs fusion bonding process described in the previous chapter (Figure 16(b)). After removing the GaAs transfer substrate and the AlGaAs etch-stop layer, a set of stripes was defined again with the orientation perpendicular ($\theta = 90°$) to the previous layer (as seen in Figure 16(c) and 16(d)).

The details of patterning process are described in the following. First, a 2000 Å-thick SiO_2 layer was deposited on the GaAs sample surface by plasma enhanced chemical vapor deposition (PECVD). Good quality of SiO_2 was obtained with following deposition conditions: deposition temperature of 275 °C, RF power of 13 watt, chamber pressure of 390 mTorr, a mixed gas of N_2O/SiH_4 (70 sccm/7.8 sccm) with a deposition rate of 280-290 Å/min. Next, the SiO_2 layer was patterned by a standard photolithography process with photoresist AZ-5209E and by wet etching in a buffered HF (BHF) solution to form the stripes. The

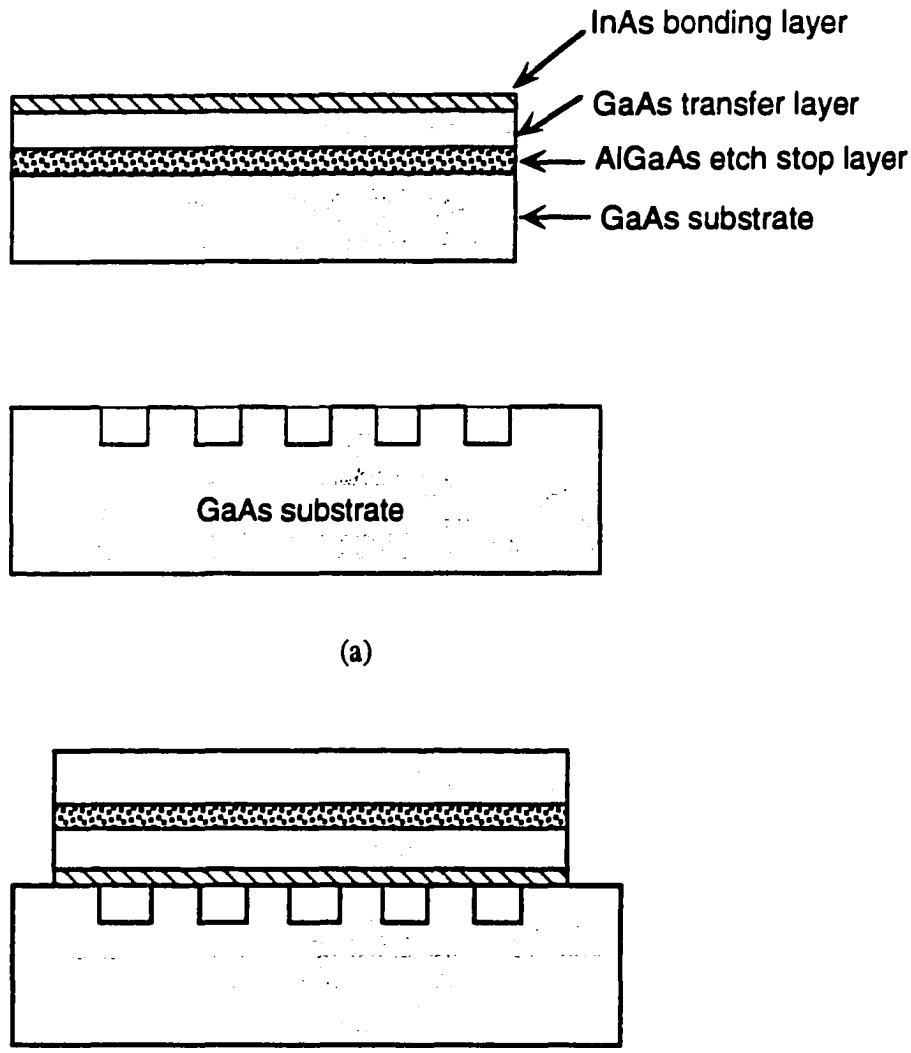

Figure 16. The schematic diagrams of fabrication process for 3-D layer-by-layer photonic band gap crystals: (a) substrate patterning and growth of epitaxial layers, (b) fusion bonding at 650 °C for 5 hours, (c) GaAs substrate and AlGaAs etch-stop layer removal after fusion bonding, (d) second PBG layer patterning with orientation rotated by 90°, (e) repeating the processes and forming a 3-layer structure, and (f) one unit cell of PBG crystal.

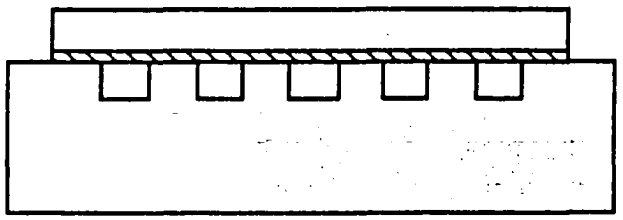

(c)

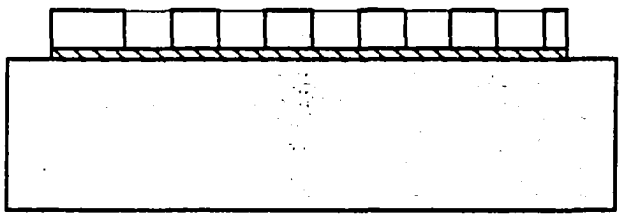

(d)

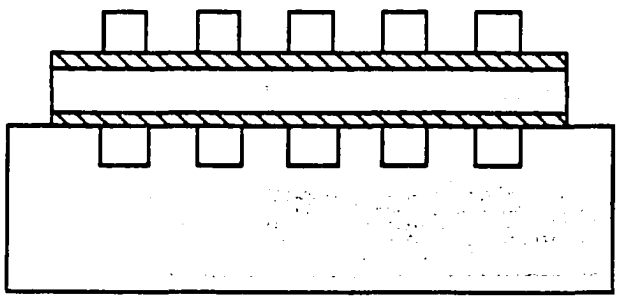

(e)

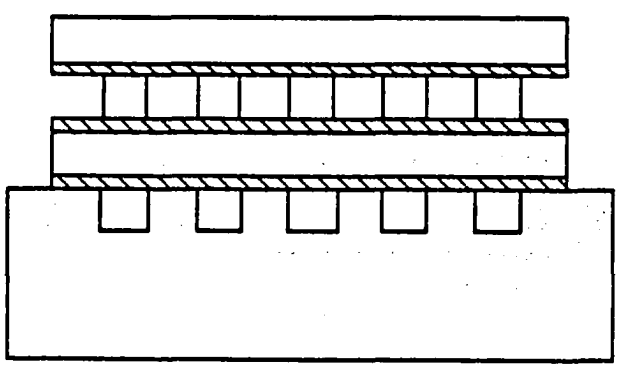

(f)

Figure 16. Fabrication process for 3-D photonic band gap crystals (continued).

resulting SiO_2 bar width was controlled by the lateral etching in BHF, and could be adjusted with SiO_2 layer thickness and etch times. Finally, PBG patterns were transferred to GaAs layer by chloride-based RIE process with SiO_2 layer as a mask. The RIE process used a gas mixture of $BCl_3/Cl_2/Ar$, giving an almost vertical etch profile as shown in Figure 15(a). Table 2 lists the RIE conditions for GaAs material. The choice of RIE parameters and their effects on etch profiles and etch selectivity are discussed in Appendix C.

Table 2. GaAs etching conditions in chloride-based RIE system.

	RIE Conditions
RF Power	100 watt
Chamber Pressure	10 mTorr
Temperature	10 °C
Mixed gas flow	$BCl_3/Cl_2/Ar$ = 10/2/8 sccm
Etch rate for GaAs	530 Å/min.
Etch rate for SiO_2	42 Å/min.

The third PBG layer was built by the same fabrication process and the stripe pattern was aligned to the first layer but shifted by half a repeat distant, d/2, in the x-y plane (Figure 16(e)). For small filling ratio structure ($f = w/d < 0.3$), bonding to the grid patterned two-layer structure required an uncovered patterned area. This step was done by shifting the top layer to provide a gas-venting path during the heating process to ensure a stable bonding without any bubbles on the bonded surfaces. The other issue was involved with alignment for the complex PBG geometry. Since GaAs material is not transparent in visible light, an alignment scheme was designed which used alignment marks on the GaAs target substrate, as well as using

smaller top bonding layers to expose the marks. The process cycle repeats every four layers, which is one unit cell in our FCT structure (Figure 16(f)). Four to six PBG layers would provide ~20 dB of attenuation inside the band gap — high enough for use in many optoelectronic devices. The process details are presented in Appendix D.

V.2. Results and Discussion

V.2.1. Multi-layered structures

Prior to the fabrication of the layer-by-layer PBG crystal operating at 10 μm, a structure with larger dimensions was tested in order to debug the process. Figure 17 shows an SEM image of a cross-sectional view of a stacked three-layer structure (bar width = 8 μm, repeat distance = 12 μm, GaAs layer = 1.25 μm, and InAs bonding layer = 0.05 μm). A structure with these dimensions would not show a photonic band gap in any frequency range since the

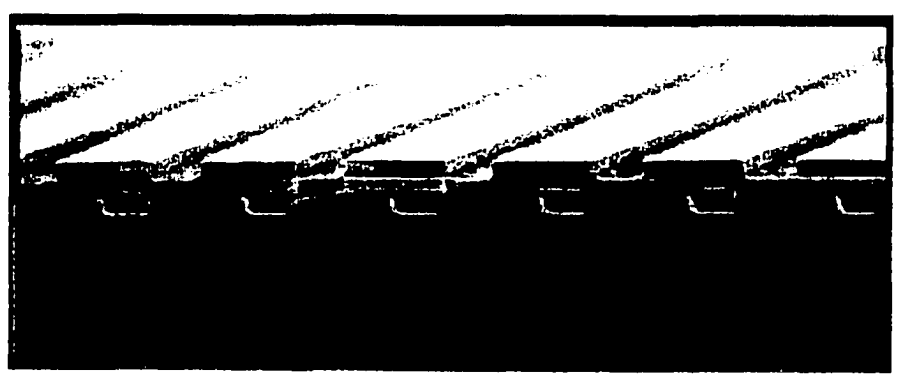

Figure 17. A SEM cross-sectional view of a stacked three-layer periodic structure with the GaAs bar width of 8 μm, repeat distant of 12 μm, GaAs layer thickness of 1.25 μm, and InAs of 0.05 μm.

dielectric filling ratio (f = w/d = 0.67) is too large and lattice constant ratio (c/a < 0.3) is too small (see Figure 4), but the developed process is applicable to structures with smaller dimensions.

Subsequently, we stacked up three layers with 1-μm feature sizes for PBG crystals operating around 10 μm. Figure 18 shows the SEM cross-sectional view of one-layer PBG structure, which was fabricated in an RIE system with a gas mixture of $BCl_3/Cl_2/Ar$. The etching conditions and gas flows used are listed in Table 2. The top views of a two-layer and three-layer structures with bar width of 0.8 μm, repeat distance of 4 μm, layer thickness of 1.0 μm, InAs thickness of 0.06 μm, and filling ratio of ~0.2 are presented in Figure 19 and 20, respectively. Note that due to process variation, the parallel bar widths from different layers are not the same (see in Figure 20).

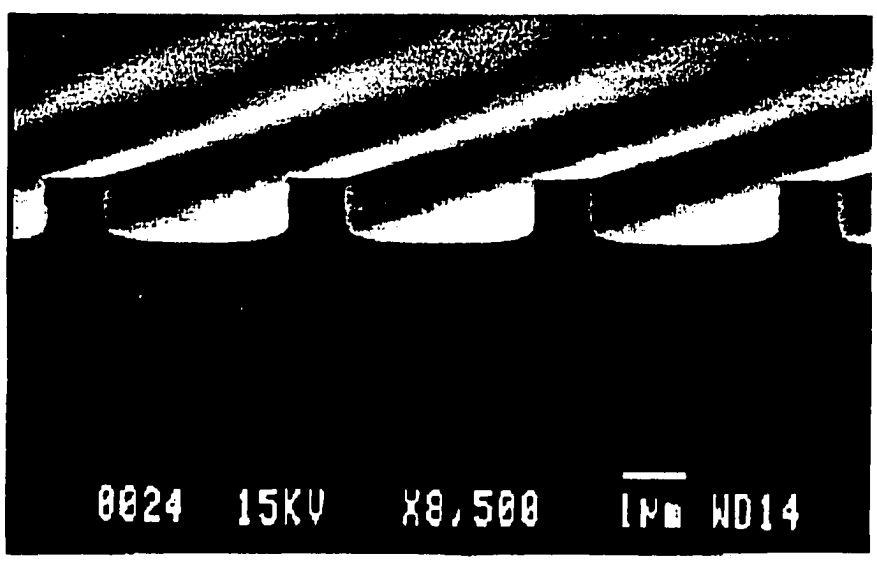

Figure 18. A SEM cross-sectional view of one-layer photonic band gap structure.

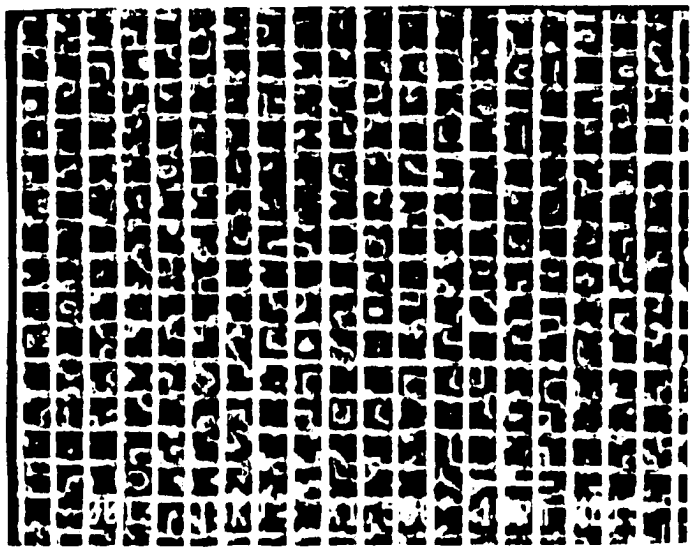

Figure 19. A SEM top view of a two-layer structure with structural dimensions for PBG crystals operating around 10 μm (bar width = 0.8 μm, repeat distant = 4 μm, GaAs layer thickness = 1.0 μm, and InAs thickness = 0.06 μm).

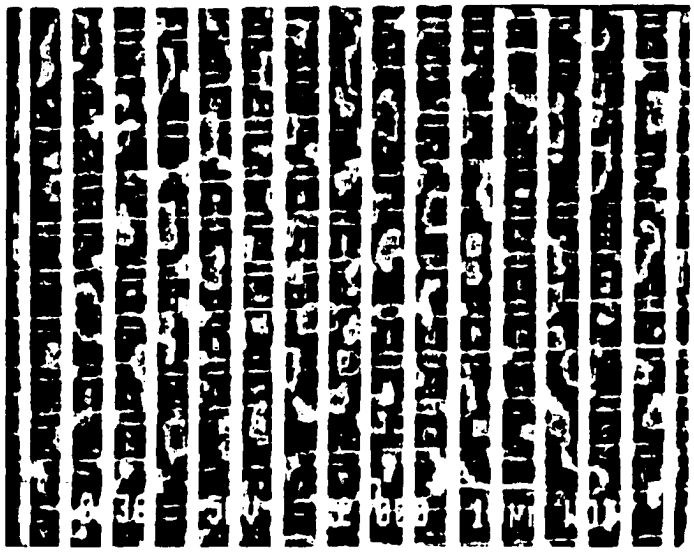

Figure 20. A SEM top view of a three-layer structure.

The GaAs PBG layer used in fabrication process was approximately 0.2 μm thinner than the designed layer thickness of 1.20 μm due to MBE growth variation. Photonic band structure calculations find that a thin uniform InAs bonding layer that of 5% of the bar thickness decreases the midgap frequency slightly and decreases the width of three-dimensional band gap by ≈ 30% as shown in Figure 7 [26]. Hence bonding layers that are less than 5% of the bar thickness could be acceptable.

The "debris" seen between the bars is most likely due to nonuniformly bonded interfaces and the residue from reactive ion etching of the bonded interlayers. The composition of the residue was analyzed by EDS, and it was found to contain In, Ga, and As atoms. It is well known that In metal and InAs can be etched away quickly in a HCl acid solution. However, attempts to remove the debris in HCl acid were not successful, and the shape of debris remained the same after etching for a long period of time. These results led us to believe that the debris is truly a (Ga,In)As alloy. Different etching formulas might be employed to attempt to selectively etch away the (Ga,In)As materials, and leave a clean grid pattern.

V.2.2. Optical characterization

To study these constructed three-dimensional multi-layered periodic structures and the effects of increasing PBG layers on the optical properties, transmission spectra were measured in mid-IR frequency range after each process step. For comparison, the transmission curves of a bare GaAs substrate and epilayers on transfer substrate are shown in Figure 21. Inside the graph, predicted photonic band edges are defined by arrows. The frequency band region should be centered around 1000 cm^{-1} (λ = 10 μm) with a gap/midgap ratio of ~25% in the stacking direction. It was calculated with fabricated structural dimensions — bar width w = 0.8 μm, repeat distance d = 4 μm, GaAs layer thickness, t = 1 μm, and an assumed thickness of 600 Å of the InAs interlayer — for at least one unit cell (4 layers).

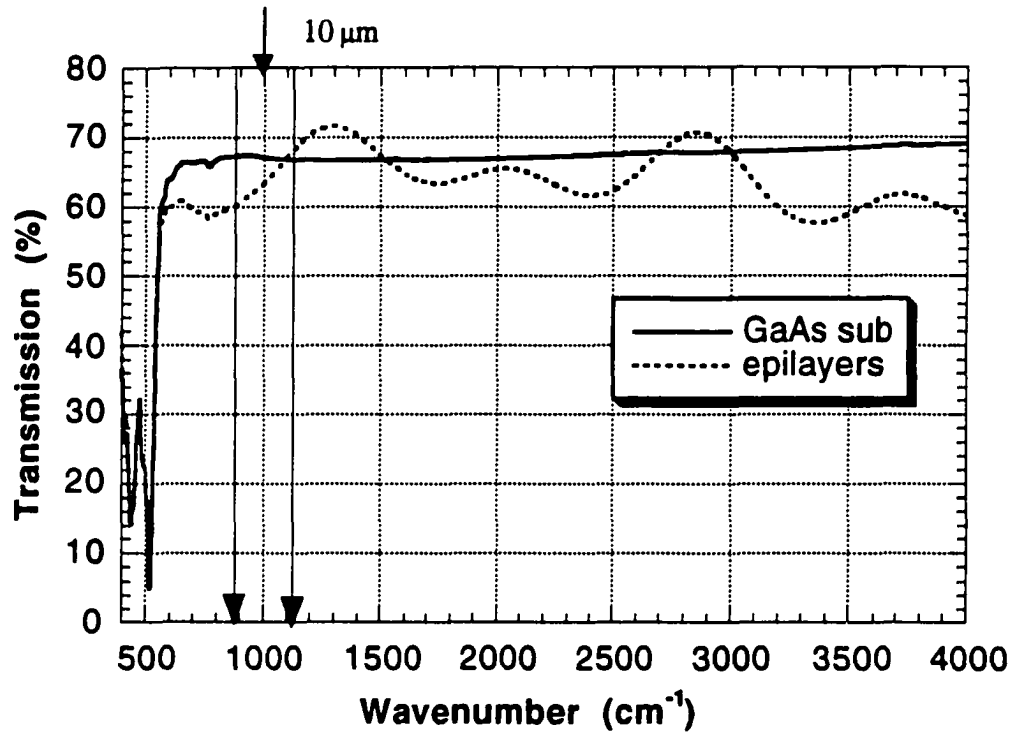

Figure 21. Measured transmission spectra of GaAs substrate and epitaxial layers on GaAs substrate (1μm of AlGaAs, 1μm of GaAs, and 0.06 μm of InAs). The arrow marks indicate the predicted photonic band edges in the stacking direction and the midgap frequency.

The transmission properties were characterized after transferring a thin GaAs layer to a patterned GaAs substrate by wafer fusion bonding and etch-back process (1.5 and 2.5 layers) and also after completing the top layer patterning (1, 2, 3, and 4 layers). Figure 22 shows the measured transmission spectra of the multi-layered periodic structures on (SI) GaAs substrates in the stacking direction. The single PBG layer is essentially a one-dimensional grating with a period of 4 μm. Adding the next PBG layer affects the optical properties significantly. The transmission measurement from a 1.5-layer structure is very similar to the one obtained from

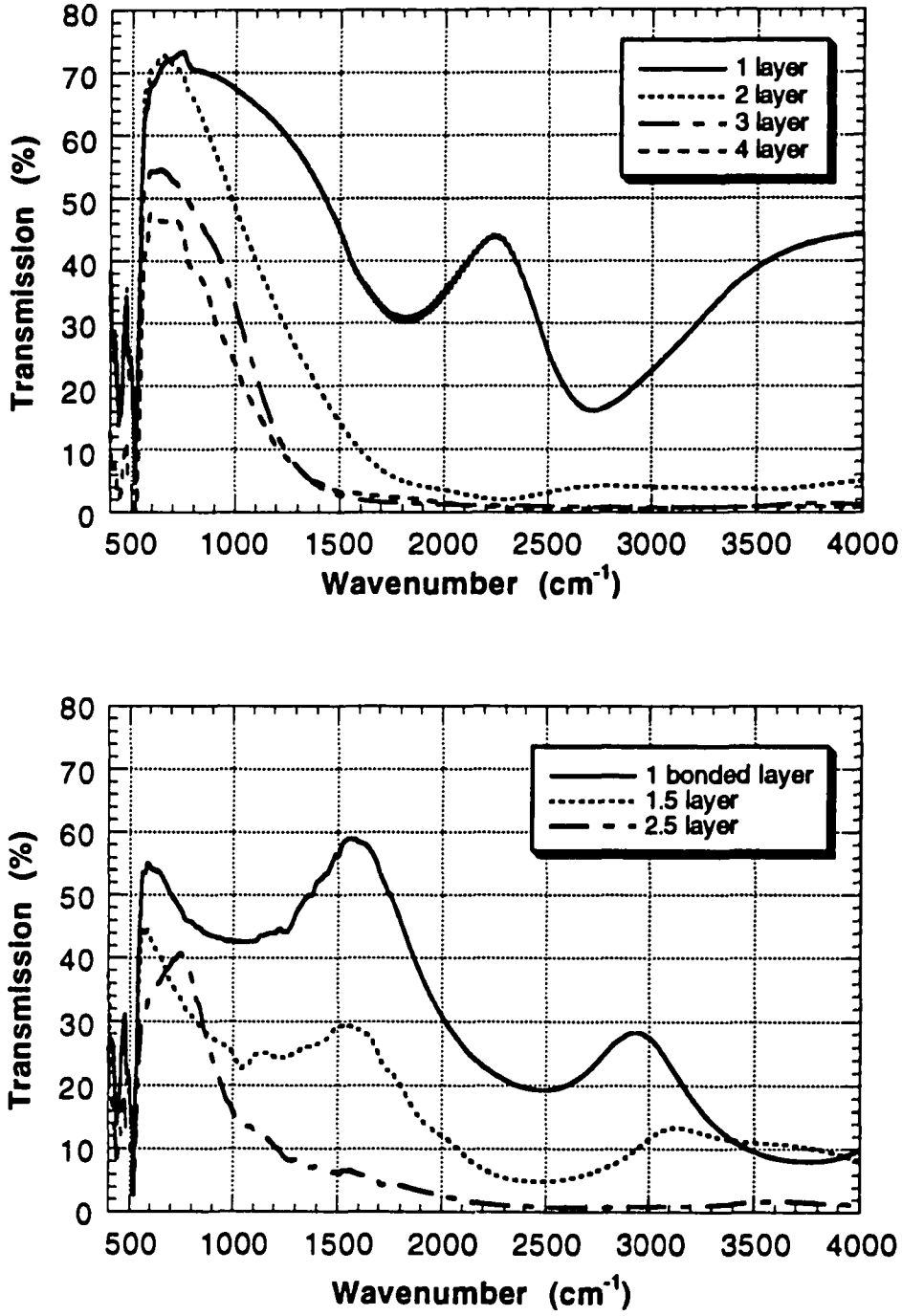

Figure 22. Measured transmission spectra of multi-layered structures after each process step.

the bare bonded layer as shown in the lower part of Figure 22. The similarity could be explained by treating the grooved layer as the scattering centers below a flat GaAs layer or by treating it as a layer with less effective dielectric constant. Once the top layer is patterned to form a grid, the transmission intensities increase back at lower frequencies, but drop dramatically above 2000 cm^{-1} from 1 to 2 layers. Note that the overall intensities of the 4-layer structure are lower as expected. The structure consists of a pair of two-layer structures, placed together with the substrate attached on each side. The parallel bars on the surfaces are perpendicular to each other without accurate alignment.

As can be seen in the whole layered spectra, the decrease in transmission becomes sharper with increasing number of PBG layers. However, the transmission intensities remain low and do not recover back in the region above the predicted upper band edge. This strong attenuation at high frequency region might be attributed by the absorption and scattering losses from each bonded interlayer. Besides, the reduced transmission from 1-dimensional grating, which might result from nonuniform etching and rough surfaces, has played a minor role.

VI. SUMMARY

We have devised a method to realize 3-D layer-by-layer PBG crystals in mid-infrared frequency range. The key step of this method is the stacking of multiple thin layers using a GaAs wafer fusion bonding technique. To enhance the bonding strength, a thin InAs film is employed as a bonding layer between two GaAs layers. With InAs layers, robust bonding as well as very smooth and uniform GaAs bonding surfaces can be achieved at ~650 °C in a flowing H_2 ambient with an uniaxial pressure of 300 g/cm^2 for annealing times ranging from 30 minutes to 5 hours. Moreover, the optical measurements of bonded flat samples show that decreasing the time for annealing clearly results in better transmission over the whole mid-IR range, particularly at higher frequencies.

For comparison, wafer bonding with a thin In metal layer has been performed under the same bonding conditions. In the InAs-based bonding, the sharp drop of transmission intensities was seen at higher frequencies. However, it has not been observed in the In metal bonding. The decrease in transmission curves over the entire spectrum seems to mainly result from the absorption losses of the In metal in mid-IR range. Also, the measured curves do not show strong dependence on annealing times.

In addition, the effects of In content on fusion bonding of $In_xGa_{1-x}As$/GaAs to GaAs substrates have been studied. Smooth and uniform surfaces are achievable for x=0.67 for a longer annealing time of 7 hours. The results of analysis show that the (Ga,In)As bonded interlayers are very similar to that obtained from InAs-based bonding. However, decreasing In content, which reduces the material absorption in (Ga,In)As layer as well as In content in bonded interlayer, effectively improves the overall transmission in mid-infrared range.

Utilizing wafer fusion bonding, selective substrate removal, and pattern etching, we have successfully built up three-layer patterned structures with PBG dimensions (~1-μm bar width, 4-μm repeat distance, and 1-μm layer thickness) that should lead to a device operating

around 10 μm. In the structure fabrication, two critical issues — venting path and alignment — have been overcome to build up several thin layers with required geometry. For stacking up patterned layers, the use of venting paths was found necessary to achieve very smooth surfaces for next layer bonding, as well as for minimizing the scattering losses from rough interfaces. Furthermore, the designed alignment scheme, which relies on the marks on GaAs target substrate and smaller bonded transfer layers, has demonstrated the capability of accuracy within 0.5 μm.

The demonstrated multi-layer periodic structures show that wafer bonding and micromachining techniques provide a feasible way to fabricate structures in a layer-by-layer fashion. With the improved bonded interfaces, the realization of 3-D PBG crystals in mid IR and possibly in the optical wavelength regime is promising.

VII. FUTURE WORK

VII.1. GaAs Fusion Bonding for 3-D PBG Crystals

The fabrication process for building up 3-D PBG layers with 1-μm feature sizes has been demonstrated using wafer fusion bonding technique in GaAs semiconductor system. However, with InAs as bonding layers, optical measurements of these bonded multi-layered structures show that the transmission intensities drop down to 5% and remain low even at frequencies above the designed band edges. This is mainly due to the scattering and absorption losses at bonded interfaces, which consist of (Ga,In)As interlayers and small voids. The losses are more pronounced in higher mid-IR region. In addition, the scattering losses could result from rough surfaces of etched patterns and nonuniform etching as well.

One way to achieve better results is to use a thin (Ga,In)As bonding layer with a 70% In content. In this case, the lower absorption of (Ga,In)As material increases the overall transmission as shown in the flat bonding, and would improve the performance in higher band edge effectively for a PBG crystal. To further realize 3-D PBG crystals, the effects of (Ga,In)As on bonding interfaces and optical characteristics need to be studied in more detail. Another obstacle for preventing the band edge recovery is related to the etched patterns in RIE system. More work needs to be done to ensure surface smoothness and uniformity of etched GaAs samples in 1-μm feature sizes.

Although (Ga,In)As alloys have been employed as bonding agents in fabrication of PBG structures in far- and mid-IR regions, the use in the materials is eventually limited in near-IR and optical regimes because of their increasing absorption with frequencies. The required thickness of a bonding layer, which provides enough In to fill in the gaps, may lead to significant reduction of photonic gap widths in higher frequency range. Besides, the size of a PBG crystal has been limited by the developed fusion process — applied high pressures,

creating a small bonded area of ~50 mm^2. For a full wafer process, the current GaAs bonding process needs to be modified to ensure a good bonding over the entire 2 inch wafer. For PBG crystals operating in frequency range > 1000 cm^{-1}, the scaled down dimensions will have bar widths in submicrons. Hence, the photolithography is no longer a suitable process. Electron beam lithography should be utilized to generate the much narrower line widths.

VII.2. Si Wafer Bonding for PBG Crystals

To overcome the scattering loss and absorption for bonding of (Ga,In)As to GaAs, effort could be directed to develop Si direct bonding technique for 3-D PBG crystals in a full wafer process. Similar to the developed process for III-V materials, a silicon on insulator (SOI) wafer can be bonded to another Si substrate using hydrophilic bonding. The Si thin film is then exposed by selective wet etching of silicon substrate and etch-stop layer (insulator). Among several types of SOI wafers, SIMOX (Separation by IMplanted OXygen) wafers have been widely used for device applications, but the prices usually are high.

A modified SOI material is then proposed to have a polycrystalline silicon thin film grown by low pressure chemical vapor deposition (PLCVD) on a SiO_2/Si substrate. Since the flatness of sample surfaces play a crucial role in Si bonding process, care should be taken in growing the poly-silicon films. In the growth process, lower temperatures are usually used to produce smoother surfaces [51]. To achieve a better bonding, the surface needs to be as flat as possible (Si surface has surface roughness of ~0.11 nm, measured by AFM). Future work should be done to investigate the effects of surface flatness and heat treatment at high temperatures on poly-Si/poly-Si bonding interfaces.

Recently, ultrathin Si wafers were introduced by the Virginia Semiconductor company. The thin silicon can be transferred to a conventional Si substrate directly using SDB with special handling techniques. The advantage of thin films is that it is flexible and can be

conformed to another surface easily. The handling problem might be overcome by gluing the thin films to a wax spun substrate which serves as a support. Once the thin film is bonded to a target substrate at room temperature, the wax might be dissolved in acetone solution, leaving the thin layer on top. In the annealing process, furnace temperatures need to be ramped up and down at an extremely slow rate to prevent the separation between the thin film and Si substrate.

Each Si bonding method mentioned above has its advantages and drawbacks. However, silicon direct bonding method is widely used and the bonding mechanism is better understood. The realization of photonic band gap crystals mainly depends on the quality of bonded interfaces. With good transmission properties from interfaces, wafer bonding is a very promising technique to fabricate 3-D layer-by-layer PBG crystals in IR and optical regimes.

APPENDIX A: WAFER FUSION BONDING FIXTURE

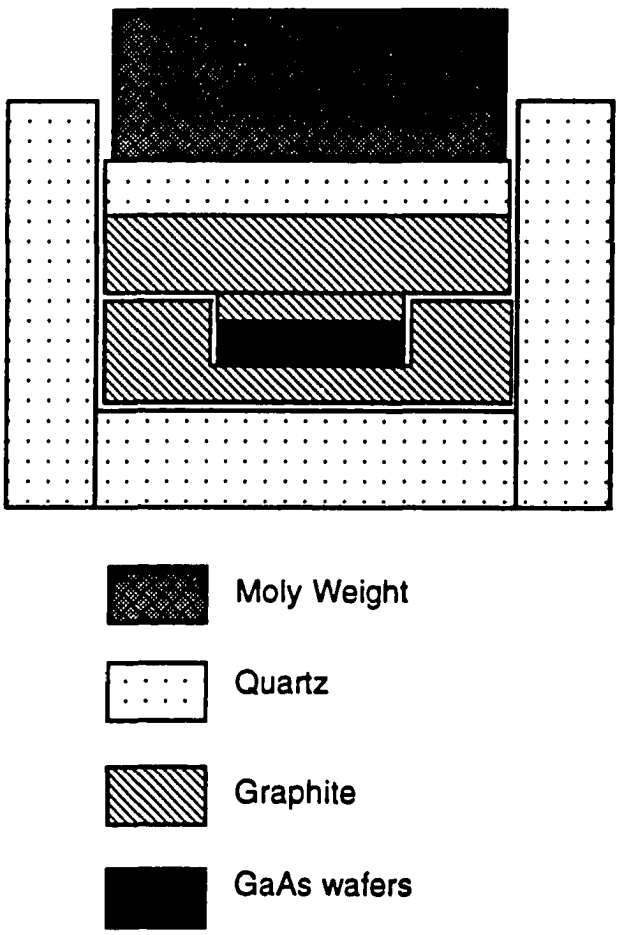

Figure A1. Schematic cross-sectional view of the apparatus for wafer fusion bonding.

APPENDIX B: FOURIER TRANSFORM INFRARED SPECTROMETER

Figure B1 [52] shows the basic FTIR spectrometer setup which consists an infrared source, IR detector, and Michelson interferometer—the main component of FTIR spectrometry. The infrared light from the source (A) is incident on the interferometer and each wavelength of light is modulated at a different frequency inside.

The operation of the reflectively scanned interferometer is outlined in the following. An incident light beam from the source is divided into two parts by striking the beamsplitter (B). About half of the light beam is reflected from beamsplitter and travels into and from the fixed mirror (C). The remaining light is transmitted through the beamsplitter and travels onto and from the moving mirror (D). When the two beams recombine, constructive or destructive interference occurs depending on the path length difference between path BC and BD.

The sinusoidally modulated beam is reflected to pass through the sample where frequency selective absorption takes place. The resulting transmitted beam reaches the detector which translates it into an electrical signal. An interferogram, which consists of the detected beam intensity as a function of movable mirror position, is generated. The interferogram has maximum magnitude at the position of zero path difference (ZPD) and is a summation of all the IR frequencies. The detector signal can not be interpreted in its original form for all practical purposes. It is converted into an IR frequency-domain spectrum by extensive computation of Fourier transformation (FT). FT determines the amplitude of each of the component signals, which gives the intensity at the corresponding frequency of light.

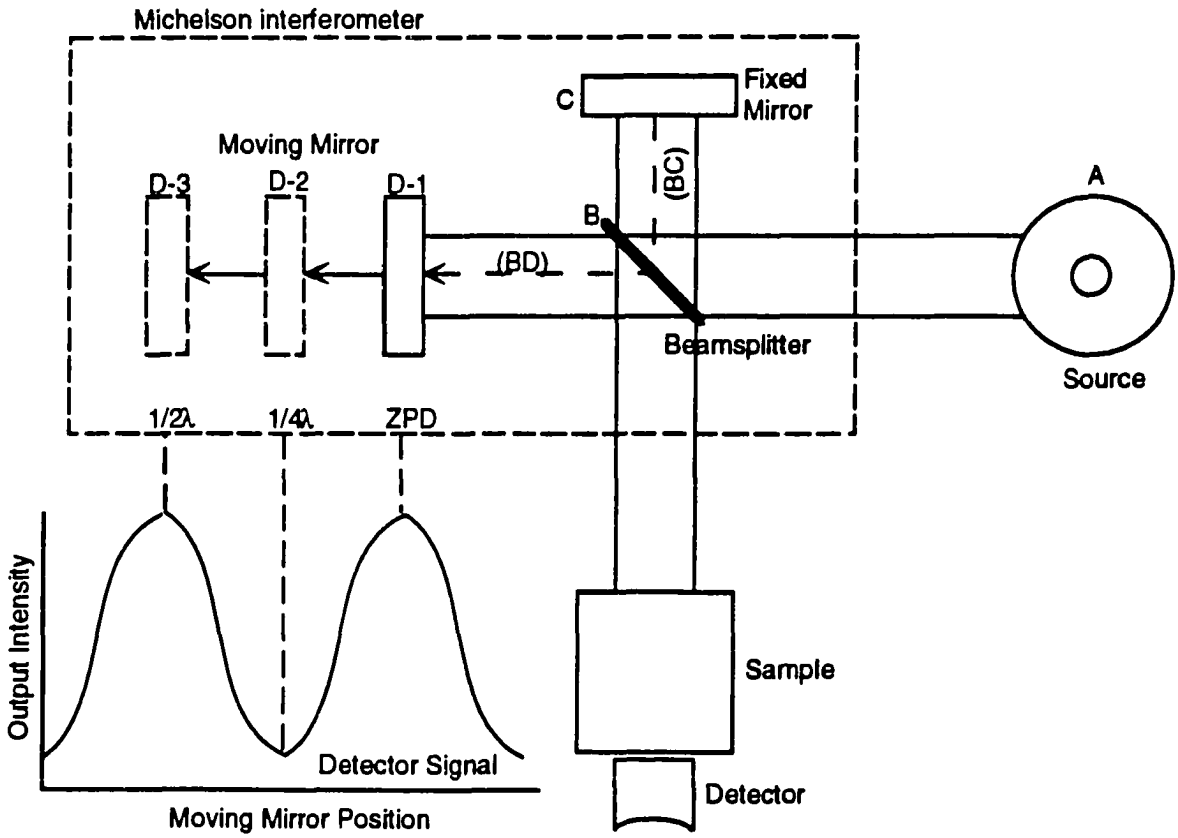

Figure B1. FTIR Spectrometer setup with source (A), beamsplitter (B), fixed mirror (C), and moving mirror (D) at positions D-1, D-2, and D-3. The output intensity as a function of mirror position is presented on the lower left corner [52].

APPENDIX C: REACTIVE ION ETCHING OF GALLIUM ARSENIDE

C.1. Dry Etching System

One of the major steps in fabrication of photonic band gap structures is to micromachine (pattern) the PBG layer by wet or dry etching. As the feature sizes become smaller, dry etching provides several advantages over wet chemical etching, such as high degree of anisotropy, smaller undercuts, and improved uniformity. Nearly vertical sidewalls can be achieved to transfer the exact dimensions from a mask in dry etching process. It is especially crucial for patterning III-V semiconductor materials, since wet etched features usually have sloped sidewalls and considerable lateral undercuts from the mask.

Dry etching methods utilize plasmas, generated by glow discharges, at low-pressure conditions (0.001-1 Torr) [53] to break the gases into energetic ions and chemical reactive radicals and molecules. Depending on the operating pressures, the etching mechanism could be a pure chemical reaction, physical effect (ion bombardment), or combination of chemical and physical effects. The reaction rates in dry etching process are limited by the concentration of reactive species and ions. The etched profiles are controlled by ion energy and reaction mechanisms. Figure C1 shows the ion energy as a function of reactor pressure and regimes for different dry etching methods [54]. The typical dry etched features associated with different etching mechanisms are demonstrated in Figure C2 [55]. Details of each etching mechanism are presented in following sections.

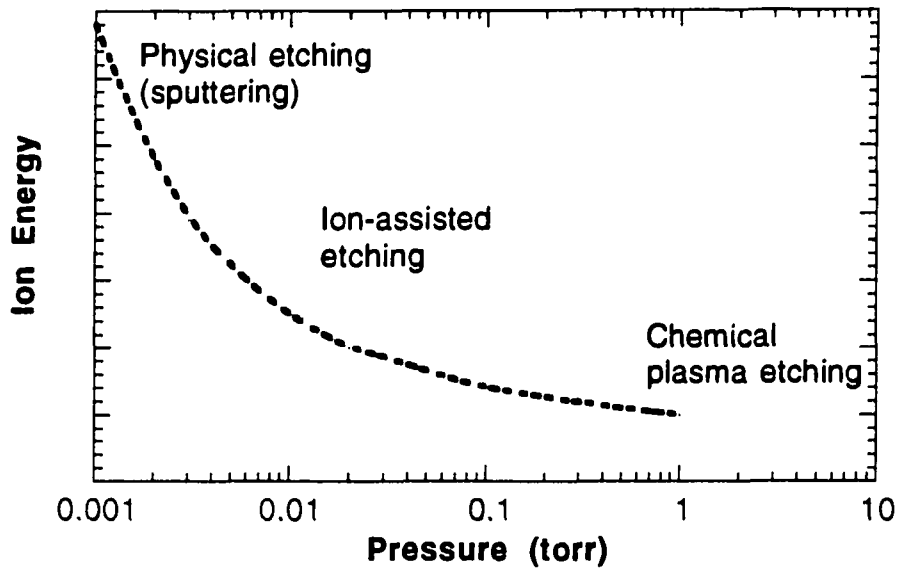

Figure C1. Ion energy vs. pressure in a plasma reactor [54].

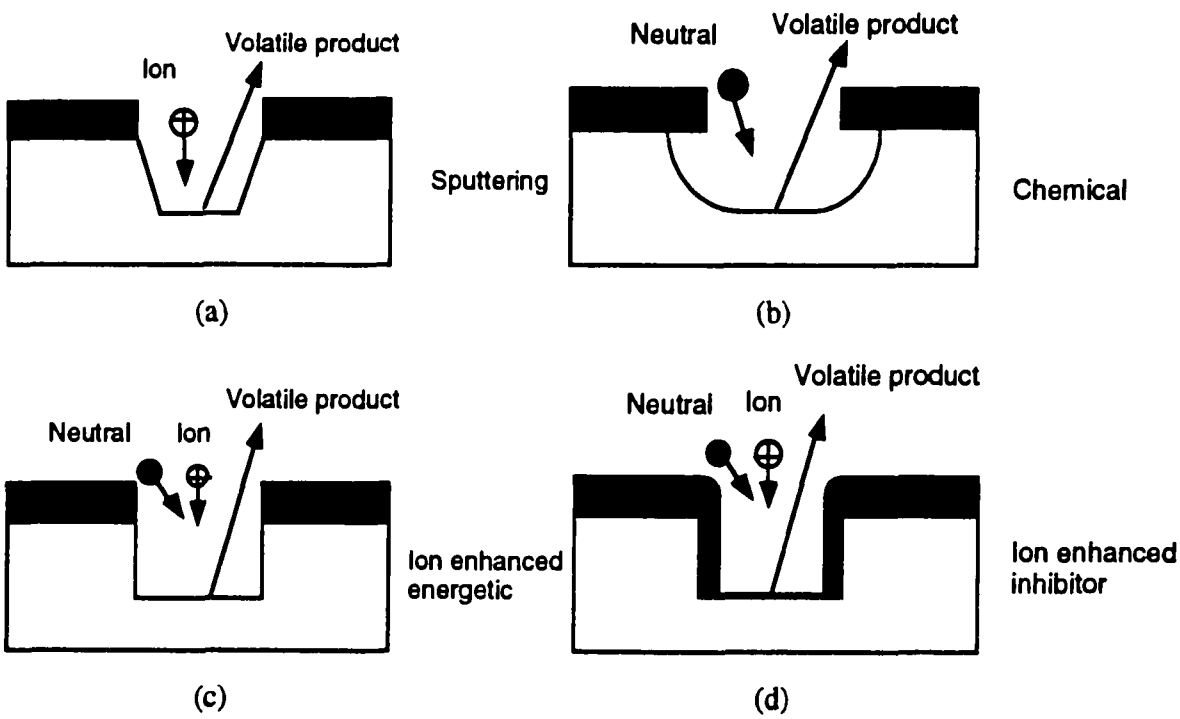

Figure C2. Dry etching profiles associated with different dry etching technique [55].

C.2. Various Dry Etching Techniques

C2.1. Plasma etching

Plasma etching occurs at relatively high pressures (0.1-1 Torr). In general, the process can be divided into six major steps [53] as shown in Figure C3. 1) Gas is initially broken down into chemically reactive species by plasma; 2) Species diffuse to the surface of substrate; 3) Species are adsorbed at surface; 4) Chemical reaction takes place; 5) The volatile reaction products are desorbed; 6) Reaction product diffuses away from the surface. In this pressure regime with low powers (voltages), neutrals are the reactive species and etching is predominated by the chemical reaction (no high energy ion bombardment due to the short mean free path length and frequent inelastic collisions). Because the neutrals arrive at the surface at random angles, the etched profile tends to be isotropic and rounded with significant undercuts. In this etching process, high etching selectivity between different materials can be obtained.

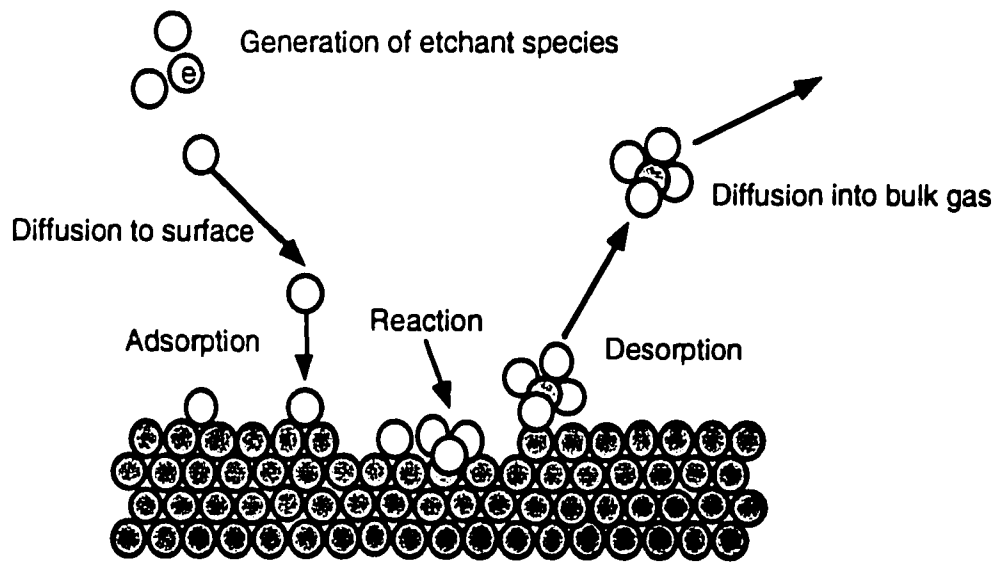

Figure C3. Chemical reaction mechanism [53].

C2.2. Sputter/ion etching

Sputter etching [53] is a purely physical phenomenon. In this technique, the reactor pressure is low, and the positive ion (for example, Ar^+) has a long mean free path, λ_i, for inelastic collision to take place. The highly energetic ions (10-5000 eV) are then accelerated from the plasma toward the target to strike the substrate at a nearly vertical angle. The momentum transfer between energetic ions and substrate surface results in breaking the chemical bonds and ballistically ejecting the substrate atoms away at a low rate (typically ~several hundreds Å/min). Consequently, sputter etching is directional and non-selective for different materials or compounds. The disadvantages of this physical etching method are that it tends to form facets and trenches. Redeposition the sputtered materials can be significant if the pressure is not low enough. Surface damage from ion bombardment can also be a problem for electronic applications.

C2.3. Reactive ion etching

Reactive ion etching is the most important dry etching method for III-V semiconductors. By changing the configuration and operating at lower pressures than plasma etching machine, RIE produces anisotropic etch profiles with good selectivity. Figure C4 shows the general configuration of a reactive ion etching system [56]. The system has a parallel-plate reactor design. The flat electrode, which holds wafers, is RF powered with a frequency of 13.6 MHz and the whole chamber wall is RF ground to enlarge the effective area. With this configuration, the voltage drop is then divided between two plasma sheaths with the following expression at low chamber pressures [56]

$$V_1/V_2 = (A_2/A_1)^4.$$

Here the V_i and A_i are the voltage drop and area of the electrodes, respectively. The large area

ratio between electrodes increases the potential difference from the plasma to the powered electrode (smaller area). The increasing energy of ion bombardment as well as the lower operation pressures (0.01-0.1 torr) enhances the directional etching compared to the plasma etching system. In RIE process, etching is dominated by ion assisted chemical reaction and ions are not the primary etching species. Therefore, it has much higher selectivity than sputter etching. Here ion assisted anisotropic etching can be achieved through different ways [53].

- Ion bombardment causes surface damage such as dangling bonds and dislocations to make a surface more reactive for the neutral plasma species.
- Ion bombardment clears the passivated surface that is coated by the reaction product, but not the protected sidewalls.
- Ion bombardment supplies the energy to drive the surface reaction.

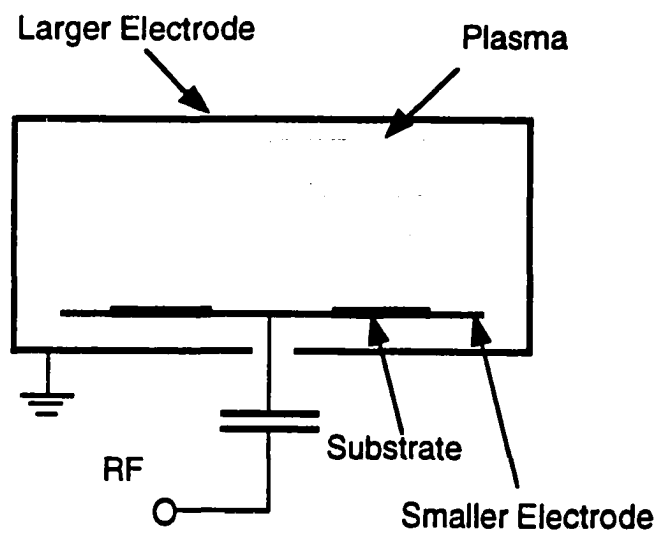

Figure C4. Schematic diagram of a reactive ion etching (RIE) system [56].

C.3. Reactive Ion Etching of GaAs

For III-V semiconductor patterning, chlorine-based plasmas are used to produce anisotropic etching profiles in reactive ion etching process. Unlike fluoride gas, Cl_2 etching is very fast in III-V materials due to its volatile etch products of III and V chlorides (except for $InCl_x$). Boron trichloride (BCl_3) has also been commonly used for GaAs (or III-V) etching because of its slower etch rate and its ability to getter water vapor [57]. More importantly, BCl_3 produces smoother etched surface by attacking the native oxide quickly and uniformly compared to Cl_2/Ar plasma etching [58]. Its smaller concentration of reactive neutral Cl and possible sidewall passivation by BCl_x increase the anisotropic effect compared to pure Cl_2 etching. Adding inert gas Argon to Cl_2 or BCl_3 slows down the fast chemical reaction and produces uniform etched surfaces. It also increases the sputtering effect of GaAs material and enhances desorption rate of weakly volatile etch products. For reactive ion etching with Cl_2-based plasmas, it has been found that SiO_2 is a better choice for masking materials over common photoresists which has a low selectivity. Due to the very fast etch of Al sample holders in Cl_2-based plasmas, the powered electrodes are covered with dummy wafers or alumina disks during the process.

Reactive etching of GaAs in BCl_3/Cl_2/Ar plasma have been investigated by changing the parameters of RF power, Cl_2 contents, process temperatures, pressures, etc [59]. The effects on selectivity, anisotropy, etch rate, and surface morphology are summarized in the following sections.

C.3.1. Effects of Cl_2 content

By varying Cl_2 fraction (15-75%) in the mixture of Cl_2/BCl_3/Ar (total flow rate, 11 sccm), the increase of GaAs etch rate with % Cl_2 has been observed [59] due to the increasing concentration of chemical reactive species. Likewise, the selectivity of etching GaAs over SiO_2

increases with increasing Cl_2 fraction. In contrast to the isotropic etching from high Cl_2 content, anisotropy of etch profiles and smoothness of etched surfaces improve significantly for a low Cl_2 content (16-40%). Same effects have been observed for changing the total flow rate but with the same fraction of Cl_2. It is mainly due to the change in Cl_2 flow rate.

C.3.2. Effects of chamber pressures

Etch rate of GaAs can be controlled by varying process pressures with a fixed plasma composition, flow rate, RF power, and process temperature as shown in Figure C5 [59]. For process temperature at ~25 °C, the etch rate peaks around 40 mTorr and decreases with the increasing pressure, which indicates the change of main etch mechanism from reactant limit to desorption limit. At higher pressures (p > 40 mTorr), the etched profiles also show severe undercuts due to the increasing collisions of ions as well as the reduction of average ion energy. In this case, ion bombardment decreases and chemical reaction is more prominent to produce isotropic etching. Similar effect has been observed for temperature of 10 °C.

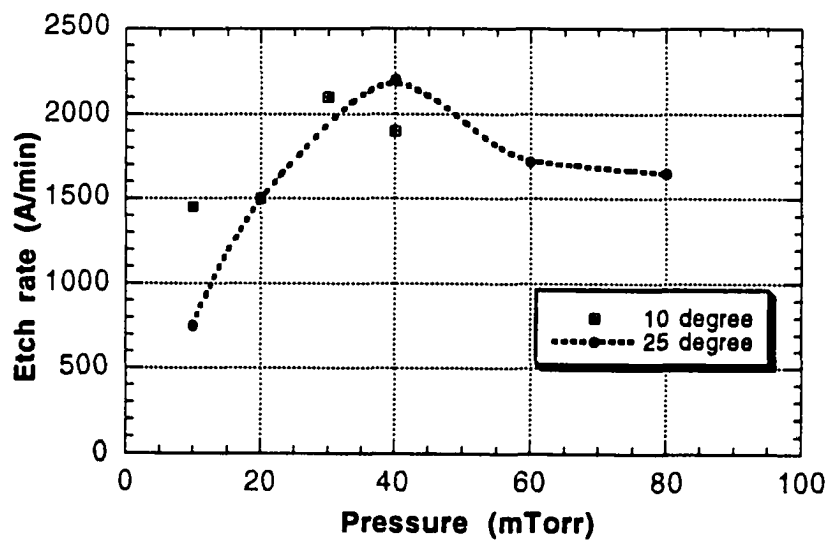

Figure C5. Etch rate as a function of process pressure for the patterned GaAs substrate with a mixed gas of $5BCl_3/2Cl_2/4Ar$, total flow rate of 11 sccm, RF power of 100 W [59].

C.3.3. Effects of process temperatures

Figure C6 [59] shows the RIE etch rate of GaAs and selectivity (etch rate ratio of GaAs/ SiO_2) as a function of process temperature with a mixed gas of $BCl_3/Cl_2/Ar$, chamber pressure of 20 mTorr, and RF power of 100 Watt. GaAs etch rate increases with chamber temperatures and reaches a maximum around 25 °C. The decreasing in etch rate for higher temperatures (> 25 °C) implies that the change of the rate-limiting step. In addition, the etch profiles show clearly the improvement of anisotropy at lower process temperatures (10-25 °C). In contrary, for high temperature etching (T > 50 °C), which is dominated by chemical reaction, significant undercuts or isotropic etch profiles are observed.

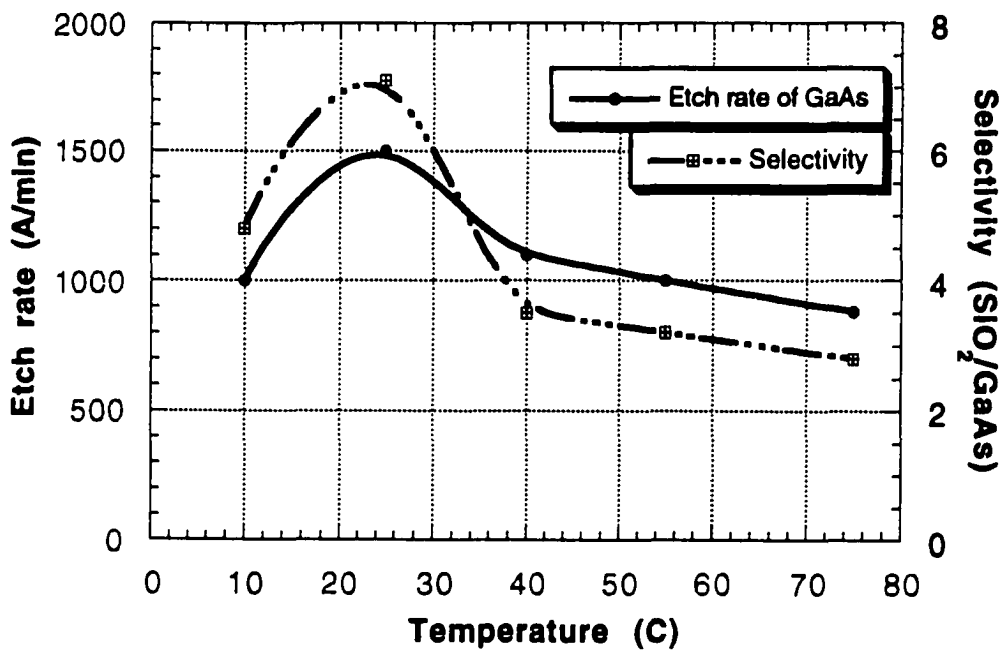

Figure C6. Etch rate as a function of temperature for the patterned GaAs substrate [59]. $BCl_3/Cl_2/Ar$ = 5/2/4, total flow rate = 11 sccm, and chamber pressure = 20 mTorr.

APPENDIX D: THREE-DIMENSIONAL PBG PROCESS

The process steps for fabrication of three-dimensional photonic band gap crystals are listed here. The process consists of 3 major steps—GaAs layer patterning, wafer fusion bonding, and GaAs substrate and etch-stop layer removal.

1. Substrate Patterning

Deposit PECVD SiO_2

SiO_2 thickness	_____
Power	13 Watt
Deposition temp.	275 °C
Chamber pressure	390 mTorr
Gas flow	N_2O:SiH_4 = 70:7.8 sccm
Deposition rate	280 Å/min.

Pattern Photoresist

Spin HMDS	5000 rpm for 10 seconds
Spin AZ-5209E	5000 rpm for 40 seconds
Expose	0.75 min.
Develop	60-70 sec.

Etch SiO_2 & Strip Photoresist

GaAs Pattern Transfer in RIE

RF power	100 Watt
Chamber pressure	10 mTorr
Process temp.	10 °C
Gas flow	BCl_3:Cl_2:Ar = 10:2:8 sccm
Etch rate	2.5 μm/40 min.

Clean SiO_2

2. Wafer Fusion Bonding

Bonding Materials	Patterned GaAs substrate & Epilayers/target substrate (~150 μm)

Bonding Pretreatment

Acetone/Methanol	5 min.
Buffered HF dip	2-5 min.
DI water rinse/Dry	5 min.

Bonding Conditions

H_2 ambient	98 sccm
Annealing temp.	650 °C
Anneal time	30 min. — 5 hours
Weight	300 g/cm^2

3. Substrate and Etch-stop Layer Removal

Etch GaAs substrate

Etching solution	Citric Acid: H_2O_2 = 4:1
Etch rate	0.4 μm/min.
Selectivity	$Al_{0.8}Ga_{0.2}As$/GaAs ~ 200

Etch AlGaAs etch-stop layer

Etching solution	HF: H_2O = 1:10
Etch time	1 μm/20 sec.

4. Second Layer Patterning

Repeat step 1

5. Third Layer Wafer Fusion Bonding

Repeat step 2. A patterned area needs to be exposed to create a venting path during the heating process.

REFERENCES

[1] E. Yablonovitch, "Inhibited spontaneous emission in solid state physics and electronics," Phys. Rev. Lett., vol. 58, pp. 2059-2062, 1987.

[2] Special issue, "Development and applications of materials exhibiting photonic band gaps," J. Opt. Soc. Amer. B, vol. 10, pp. 208-408, 1993.

[3] C. M. Soukoulis, "Photonic band gaps and localization," New York: Plenum Press, 1993.

[4] E. Yablonovitch, Gmitter, T. J., "Donor and Acceptor Modes in Photonic Band Structure," Phys. Rev. Lett., vol. 67, pp. 3380-3383, 1991.

[5] E. Yablonovitch, "Photonic band-gap structures," J. Opt. Soc. Amer. B, vol. 10, pp. 283-295, 1993.

[6] M. Scalora, Dowling, J. P., Tocci, M., Bloemer, M. J., Bowden, C. M., Haus, J. W., "Dipole emission rates in one-dimensional photonic band-gap materials," Appl. Phys. B, vol. 60, pp. S57-S61, 1995.

[7] R. D. Meade, Devenyi, A., Joannopoulos, J. D., Alerhand, O. L., Smith, D. A., Kash, K., "Novel applications of photonic band gap materials: Low-loss bends and high Q cavities," J. Appl. Phys., vol. 75, pp. 4753-4755, 1994.

[8] J. D. Joannopoulos, R. D. Meade, and J. N. Winn, *Photonic Crystals: molding the flow of light.* New Jersey: Princeton University Press, 1995.

[9] S. D. Cheng, Biswas, R., Ozbay, E., McCalmont, J. S., Tuttle, G., Ho, K. M., "Optimized dipole antennas on photonic band gap crystals," Appl. Phys. Lett., vol. 67, pp. 3399-3401, 1995.

[10] K. M. Ho, Chan, C. T. and Soukoulis, C. M., "Existence of photonic band gap in periodic dielectric structures," Phys. Rev. Lett., vol. 65, pp. 3152-3155, 1990.

[11] C. T. Chan, Ho, K. M., Soukoulis, C. M., "Photonic band-gap in experimentally realizable periodic structures," Europhys. Lett., vol. 16, pp. 563-568, 1991.

[12] E. Yablonovitch, Gmitter, T. J., Leung, K. M., "Photonic band structure: The face-centered-cubic case employing nonspherical atoms," Phys. Rev. Lett., vol. 67, pp. 2295-2298, 1991.

[13] K. M. Ho, Chan, C. T., Soukoulis, C. M., Biswas, R. and Sigalas, M., "Photonic band gaps in three dimensions: New layer-by-layer periodic structures," Solid State Comm., vol. 89, pp. 413-416, 1994.

[14] S. Fan, Villeneuve, P. R., Meade, R. D., and Joannopoulos, J. D., "Design of three dimensional photonic crystals at submicron lengthscales," Appl. Phys. Lett., vol. 65, pp. 1466-1468, 1994.

[15] C. C. Cheng, Scherer, A., "Fabrication of photonic band-gap crystals," J. Vac. Sci. Technol. B, vol. 13, pp. 2696-2700, 1995.

[16] C. C. Cheng, Arget-Engels, V., Scherer, A., Yablonovitch, E., "Nanofabricated three dimensional photonic crystals operating at optical wavelengths," Physica Scripta, vol. T68, pp. 17-20, 1996.

[17] G. Feiertag, Ehrfeld, W., Freimuth, H., Kolle, H., Lehr, H., Schmidt, M., Sigalas, M. M., Soukoulis, C. M., Kiriakidis, G., Pedersen, T., Kuhl, J., Koenig, W., "Fabrication of photonic crystals by deep x-ray lithography," Appl. Phys. Lett., vol. 71, pp. 1441-1443, 1997.

[18] E. Ozbay, Michel, E., Tuttle, G., Biswas, R., Sigalas, M., Ho, K. M., "Micromachined millimeter-wave photonic band-gap crystals," Appl. Phys. Lett., vol. 64, pp. 2059-2061, 1994.

[19] E. Ozbay, Michel, E., Tuttle, G., Biswas, R., Ho, K. M., Bostak, J., Bloom, D. M., "Double-etch geometry for millimeter-wave photonic band-gap crystals," Appl. Phys. Lett., vol. 65, pp. 1617-1619, 1994.

[20] E. Ozbay, Michel, E., Tuttle, G., Biswas, R., Ho, K. M., "Terahertz spectroscopy of three-dimensional photonic band-gap crystals," Optics Letters, vol. 19, pp. 1155-1157, 1994.

[21] M. C. Wanke, Lehmann, O., Muller, K., Wen, Q., Stuke, M., "Laser rapid prototyping of photonic band gap microstructures," in Science, vol. 275, pp. 1284-1286, 1997.

[22] S. Y. Lin, Fleming, J., Biswas, R., Sigalas, M. M., Ho, K.-M., Smith, B. K., Hetherington, D. L., Zubrzycki, W., Kurtz, S. R., Bur, J., "A three-dimensional photonic crystal in the infrared wavelengths," accepted in Nature, 1998.

[23] S. G. Romanov, Johnson, N. P., Fokin, A. V., Butko, V. Y., Yates, H. M., Pemble, M. E., Sotomayor Torres, C. M., "Enhancement of the photonic gap of opal-based three-dimensional gratings," Appl. Phys. Lett., vol. 70, pp. 2091-2093, 1997.

[24] R. Biswas, Ozbay, E., Ho, K.-M., "Photonic band gaps with layer-by-layer double etched structures," J. Appl. Phys., vol. 80, pp. 6749-6753, 1996.

[25] K.-M. Ho, Chan, C. T., Soukoulis, C. M., Biswas, R. and Sigalas, M., private communication.

[26] R. Biswas, private communication.

[27] E. D. Palik, Ed., *Handbook of optical constants of solids* New York: Academic Press, 1985.

[28] E. D. Palik, Ed., *Handbook of optical constants of solids II* San Diego: Academic Press, 1991.

[29] E. Ozbay, Abeyta, A., Tuttle, G., Tringides, M., Biswas, R., Chan, C. T., Soukoulis, C. M., Ho, K.-M., "Measurement of a three-dimensional photonic band gap in a crystal structure made of dielectric rods," Phys. Rev. B, vol. 50, pp. 1945-1948, 1994.

[30] M. Shimbo, K. Furukawa, K. Fukuda, and K. Tanzawa, "Silicon-to-silicon direct bonding method," J. Appl. Phys., vol. 60, pp. 2987-2989, 1986.

[31] R. Stengl, K.-Y. Ahn, and U. Gosele, "Bubble-Free Silicon Wafer Bonding in a Non Cleanroom Enviroment," Jpn J. Appl. Phys., vol. 27, pp. L2364-2366, 1988.

[32] K. Liungberg, A. Soderbarg, and Y. Backlund, "Spontaneous bonding of hydrophobic silicon surfaces," Appl. Phys. Lett., vol. 62, pp. 1362-1364, 1993.

[33] Q.-Y. Tong, E. Schmidt, and U. Gosele, "Hydrophobic silicon wafer bonding," Appl. Phys. Lett., vol. 64, pp. 625-627, 1994.

[34] E. Yablonovitch, Hwang, D. M., Gmitter, T. J., Florez, L. T., Harbison, J. P., "Van der Waals bonding of GaAs epitaxial liftoff films onto arbitrary substrates," Appl. Phys. Lett., vol. 56, pp. 2419-2421, 1990.

[35] E. Yablonovitch, Sands, T., Hwang, D. M., Schnitzer, I., Gmitter, T. J., Shastry, S. K., Hill, D. S., Fan, J. C. C., "Van der Waals bonding of GaAs on Pd leads to a permanent, solid-phase-topotaxial, metallurgical bond," Appl. Phys. Lett., vol. 59, pp. 3159-3161, 1991.

[36] I. H. Tan, Reaves, C., Dudley, J. J., Holmes, A. L., Babic, D. I., Hu, E. L., Bowers, J. E., Denbaars, S., "Low-temperature Pd direct bonding and electrical transport across InP-Pd-GaAs interfaces," in Proc. 6th Intl. Conference on InP and Related Materials, paper ThG46, 1994.

[37] R. Venkatasubramanian, M. L. Timmons, T. P. Humphreys, B. M. Keyers, and R. K. Ahrenkiel, "High-quality eutectic-metal-bonded AlGaAs-GaAs thin films on Si substrates," Appl. Phys. Lett., vol. 60, pp. 886-888, 1992.

[38] K. W. Goossen, J. E. Cunningham, and W. Y. Jan, "GaAs 850 nm modulators solder-bonded to silicon," IEEE Photonics Technol. Lett., vol. 5, pp. 776-778, 1993.

[39] Z. L. Liau, Walpole, J. N., Tsang, D. Z., "Fabrication, characterization, and analysis of mass-transported GaInAsP/InP buried heterostructure lasers," IEEE J. Quantum Electron., vol. QE-20, pp. 855, 1984.

[40] Z. L. Liau and D. E. Mull, "Wafer fusion: A novel technique for optoelectronic device fabrication and monolithic integration," Appl. Phys. Lett., vol. 56, pp. 737-739, 1990.

[41] Y. H. Lo, R. Bhat, D. M. Hwang, M. A. Koza, and T. P. Lee, "Bonding by atomic rearrangement of InP/InGaAsP 1.5 μm wavelength lasers on GaAs substrates," Appl. Phys. Lett., vol. 58, pp. 1961-1963, 1991.

[42] J. J. Dudley, M. Ishikawa, D. I. Babic, B. I. Miller, R. Mirin, W. B. Jiang, J. E. Bowers, and E. L. Hu, "144 C operation of 1.3 μm InGaAsP vertical cavity lasers on GaAs substrates," Appl. Phys. Lett., vol. 61, pp. 3095-3097, 1992.

[43] D. I. Babic and J. J. Dudley, "Double-fused 1.52-μm vertical-cavity lasers," Appl. Phys. Lett., vol. 66, pp. 1030-1032, 1995.

[44] I.-H. Tan, J. J. Dudley, D. I. Babic, D. A. Cohen, B. D. Young, E. L. Hu, J. E. Bowers, B. I. Miller, U. Koren, and M. G. Young, "High quantum efficiency and narrow absorption bandwidth of the wafer-fused resonant $In_{0.53}Ga_{0.47}As$ photodetectors," IEEE Photonics Technol. Lett., vol. 6, pp. 811-813, 1994.

[45] F. A. Kish, F. M. Steranka, D. C. DeFevere, D. A. Vanderwater, K. G. Park, C. P. Kuo, T. D. Osentowski, M. J. Peanasky, J. G. Yu, R. M. Fletcher, D. A. Steigerwald, M. G. Craford, and V. M. Robbins, "Very high-efficiency semiconductor wafer-bonded transparent-substrate $(Al_xGa_{1-x})_{0.5}In_{0.5}P$/GaP light-emitting diodes," Appl. Phys. Lett., vol. 64, pp. 2839-2841, 1994.

[46] L. Gordon, Wood, G. L., Eckardt, R. C., Route, R. R., Feigelson, R. S., Fejer, M. M., Byer, R., "Diffusion-bonded stacked GaAs for quasiphase-matched second-

harmonic generation of a carbon dioxide laser," Electron. lett., vol. 29, pp. 1942-1944, 1993.

[47] S. J. B. Yoo, R. Bhat, C. Caneau, and M. A. Koza, "Qusi-phase-matched second-harmonic generation in AlGaAs waveguides with periodic domain inversion achieved by wafer-bonding," Appl. Phys. Lett., vol. 66, pp. 3410-3412, 1995.

[48] Y. H. Lo, R. Bhat, D. M. Hwang, C. Chua, and C.-H. Lin, "Semiconductor lasers on Si substrates using the technology of bonding by atomic rearrangement," Appl. Phys. Lett., vol. 62, pp. 1038-1040, 1993.

[49] A. R. Hawkins, T. E. Reynolds, D. R. England, D. I. Babic, M. J. Mondry, K. Streubel, and J. E. Bowers, "Silicon heterointerface photodetector," Appl. Phys. Lett., vol. 68, pp. 3692, 1996.

[50] F. E. Ejeckam, Seaford, M. L., Lo, Y.-H., "Dislocation-free InSb grown on GaAs compliant universal substrates," Appl. Phys. Lett., vol. 71, pp. 776-778, 1997.

[51] M. Madou, "Surface Micromachining," in *Fundamentals of microfabrication*, New York: CRC Press, 1997, pp. 217-274.

[52] "*Magna-IR FT-IR Spectrometer: System 560 and 760 User's Guide*," Nicolet Instrument Corporation, 1996.

[53] M. Madou, "Pattern transfer with dry etching techniques," in *Fundamentals of microfabrication*, New York: CRC Press, 1997, pp. 53-88.

[54] D. L. Flamm, "Dry plasma resist stripping: overview of equipment," Solid State Technol., vol. 35, pp. 37-39, 1991.

[55] D. L. Flamm, "Feed gas purity and environmental concerns in plasma etching," Solid State Technol., vol. 36, pp. 49-54, 1993.

[56] R. Williams, "Dry etching—plasma, RIE, RIBE, ion milling," in *Modern GaAs processing methods*. Norwood: Artech House, 1990, pp. 173-195.

[57] H. B. Bell, Anderson, H. M., Light, R. W., "Reactive ion etching of aluminum/silicon in BBr_3/Cl_2 and BCl_3/Cl_2 Mixture," Science and Technology, vol. 135, pp. 1184-1191, 1988.

[58] S. J. Pearton, Abernathy, C. R., Kopf, R. F., Ren, F., "Low temperature chlorine-based dry etching of III-V semiconductors," J. Electrochem. Soc., vol. 141, pp. 2250-2256, 1994.

[59] F. Olympie, private communication.

ACKNOWLEDGMENTS

I would like to thank my major professor, Dr. Gary Tuttle, for supporting me in this project which has proven to be very interesting. I would also like to thank his guidance and assistance throughout this project and my graduate study at Iowa State University.

Special thanks to my committee members, Dr. Kai-Ming Ho for his support and insightful comments, Dr. C. Hsieh and Dr. Robert Weber for their time and encouragement, and Dr. Rana Biswas for providing me all the theoretical calculations in the projects and for his helpful discussion.

Thanks also go to Allen Landin for his assistant of PECVD process, Warren Straszherm for his help with EDS analysis, and Florence Olympie for her work in RIE.

I would also like to thank all my friends and colleagues at Microelectronics Research Center, Sandhya Gupta, Jonathan Kavanaugh, Wai Leung, Phillip, Russ, Jason, Karl, Kay Han, Ruth Shinar and all the others for their help, as well as for providing a more enjoyable environment to work in.

IMAGE EVALUATION
TEST TARGET (QA-3)

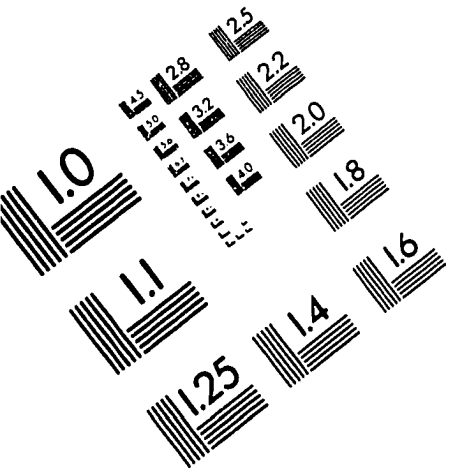

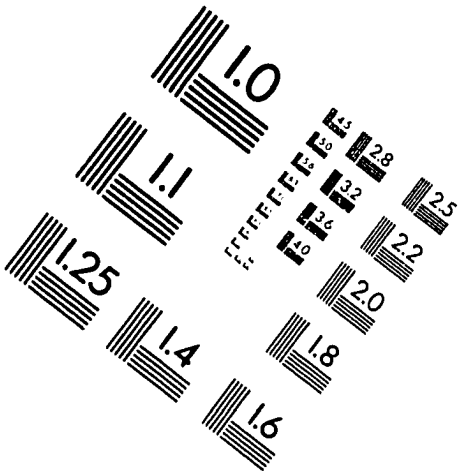

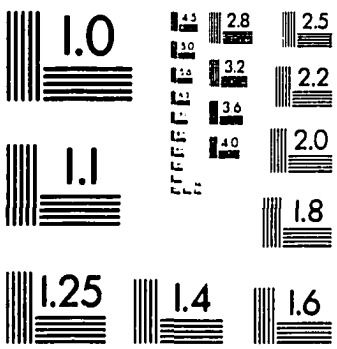

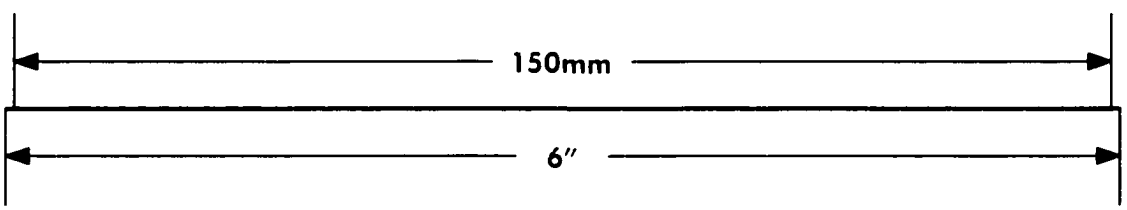

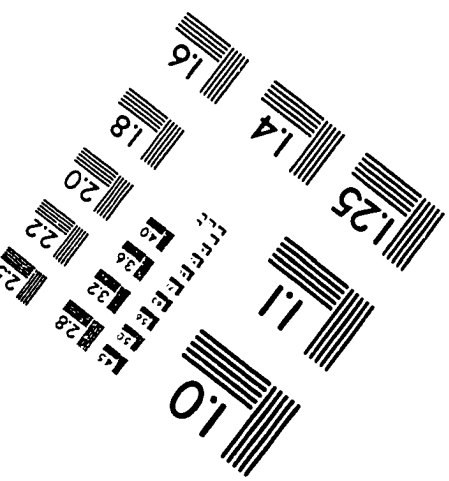

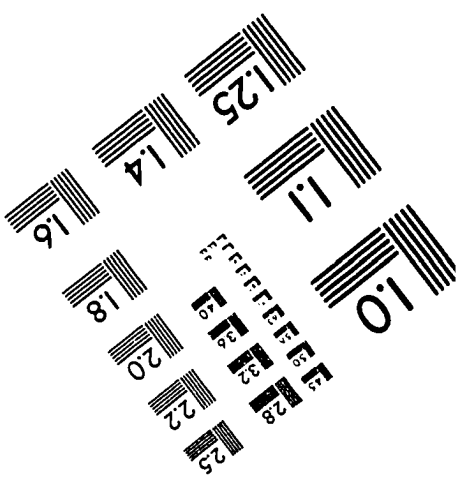

APPLIED IMAGE, Inc
1653 East Main Street
Rochester, NY 14609 USA
Phone: 716/482-0300
Fax: 716/288-5989